Evolutionary dynamics with fluctuating population sizes and strong mutualism

Thiparat Chotibut and David R. Nelson

Phys. Rev. E **92**, 022718 — Published 20 August 2015

DOI: 10.1103/PhysRevE.92.022718

Evolutionary Dynamics with Fluctuating Population Sizes and Strong Mutualism

Thiparat Chotibut* and David R. Nelson†
Department of Physics, Harvard University, Cambridge, Massachusetts 02138, USA

Game theory ideas provide a useful framework for studying evolutionary dynamics in a well-mixed environment. This approach, however, typically enforces a strictly fixed overall population size, deemphasizing natural growth processes. We study a competitive Lotka-Volterra model, with number fluctuations, that accounts for natural population growth and encompasses interaction scenarios typical of evolutionary games. We show that, in an appropriate limit, the model describes standard evolutionary games with both genetic drift and overall population size fluctuations. However, there are also regimes where a varying population size can strongly influence the evolutionary dynamics. We focus on the strong mutualism scenario and demonstrate that standard evolutionary game theory fails to describe our simulation results. We then analytically and numerically determine fixation probabilities as well as mean fixation times using matched asymptotic expansions, taking into account the population size degree of freedom. These results elucidate the interplay between population dynamics and evolutionary dynamics in well-mixed systems.

PACS numbers: 87.18.Tt, 87.23.Kg, 05.10.Gg, 05.40.-a
Keywords: evolutionary game theory, population genetics, fluctuating population sizes, noise-induced phenomena, stochastic non-linear dynamics

I. INTRODUCTION

Recent advances in experimental evolution open new directions for quantitative studies of evolutionary dynamics [1, 2]. In a well-mixed environment such as a chemostat or a shaken test tube, the relative frequency of interacting microbes can be measured over time. Although microbial experiments demonstrate an intricate feedback between evolutionary and population dynamics [3–5], theoretical understanding is often limited to evolutionary dynamics in a fixed population size, mostly within the framework of evolutionary game theory and population genetics [6–12].

In a well-mixed system with infinitely large populations, evolutionary game theory prescribes deterministic time evolution of the relative frequency $f_i(t)$ of species i by the replicator dynamics:

$$\frac{df_i}{dt} = [w_i(\boldsymbol{f}) - \bar{w}(\boldsymbol{f})]\, f_i, \tag{1}$$

where $w_i(\boldsymbol{f})$ is the frequency-dependent fitness of species i , and $\bar{w}(\boldsymbol{f}) = \sum_j f_j w_j(\boldsymbol{f})$ is the mean fitness of all interacting species [6, 7, 13]. The replicator dynamics encapsulate frequency-dependent natural selection: a fitter species flourishes and a weaker species succumbs to evolutionary forces. The fitness of species i is often defined as a constant background plus the total payoff from interactions, assumed to be linear in the $\{f_i(t)\}$, $w_i(\boldsymbol{f}) = 1 + \sum_j a_{ij} f_j$, where a_{ij} is a phenomenological payoff matrix characterizing interactions with species j. For two interacting species, which is typical in a competition experiment [1, 2] and is the focus of this paper, the frequency $f(t)$ of species 1 fully specifies the state of evolutionary dynamics, since the frequency of species 2 is just $1 - f(t)$. In this case, the replicator dynamics determines the time evolution of $f(t)$ from Eq. (1) as

$$\begin{aligned} \frac{df}{dt} &= [\alpha_1 - (\alpha_1 + \alpha_2)f](1-f)f, \\ &\equiv v_E(f), \end{aligned} \tag{2}$$

where $\alpha_1 = a_{12} - a_{22}$ and $\alpha_2 = a_{21} - a_{11}$.

A rich variety of competition scenarios emerge from this simple description of evolutionary games. Depending on the payoff differences α_1 and α_2, Eq. (2) exhibits 5 qualitatively different competition scenarios, schematically sketched in Fig. 1 [6, 7]. For positive α's (first quadrant of Fig. 1), a stable fixed point corresponding to a species coexistence appears at $f^* = \alpha_1/(\alpha_1 + \alpha_2)$, lying between the unstable fixed points $f = 0$ and $f = 1$. This scenario is commonly referred to as the "snowdrift game" in game theory or *mutualism* in the context of evolution [7, 14, 15]. For negative α's (third quadrant of Fig. 1), the fixed point f^* becomes unstable while the fixed points with f equals 0 and 1 are stable. This bistability situation is known by "coordination game" in game theory or *antagonism* in our context. When α's have opposite signs (second quadrant and fourth quadrant of Fig. 1), scenarios in game theory are either called "harmony" or "prisoner's of the dilemma". In this case, either f^* or $1 - f^*$ exceed unity, and the fixed point f^* becomes inaccessible. The only relevant fixed points are $f = 0$ and $f = 1$ and only one of them is stable: For $\alpha_1 > 0$ and $\alpha_2 < 0$, the fixed point $f = 1$ is stable and species 1 dominates, i.e., fixes at 100% of the population at long times. For $\alpha_2 > 0$ and $\alpha_1 < 0$, the fixed point $f = 0$ is stable and species 2 dominates. Lastly, at the

* Electronic address: thiparatc@gmail.com
† Electronic address: nelson@physics.harvard.edu

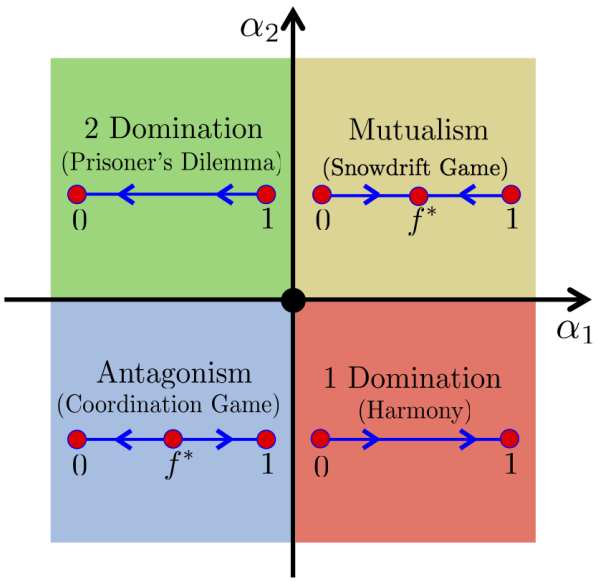

FIG. 1. (Color online) Four competition scenarios in the replicator dynamics represented by the four quadrants. The fifth scenario, neutral evolution ($\alpha_1 = \alpha_2 = 0$), in which every point $f \in [0, 1]$ is a fixed point, arises at the origin.

origin of Fig. 1, when $\alpha_1 = \alpha_2 = 0$, every point is a fixed point. We shall refer to this fixed line scenario as *neutral evolution*, representing situations when the two interacting species are neutral variants of each other.

In finite populations, however, evolutionary dynamics are not only influenced by deterministic frequency-dependent selection term $v_E(f)$, but also by randomness due to discrete microscopic birth and death events, commonly referred to as number fluctuations or genetic drift in population genetics [9–11, 16]. Evolutionary game theory in a strictly fixed population size can be reformulated to account for genetic drift, with equations that reduce to the deterministic replicator dynamics in the limit of infinitely large population size [6, 7]. For a fixed population size $N \gg 1$ and weak payoffs $|a_{ij}| \ll 1$, the continuum approximation of replicator dynamics with genetic drift reads

$$\frac{df}{dt} = v_E(f) + \sqrt{\frac{2D_g(f)}{N}}\Gamma(t), \qquad (3)$$

where $\Gamma(t)$ is a zero-mean Gaussian white-noise with a unit variance, and $D_g(f)/N = f(1-f)/N$ is the frequency-dependent noise amplitude describing the discrete birth and death processes [14]. In population genetics, the stochastic differential equation (3) must be interpreted according to Ito's prescription [14, 17], which we shall assume also for all noise terms appearing in this manuscript. For neutral evolution, $v_E(f) = 0$ and the dynamics is equivalent to the continuum limit of the Wright-Fisher sampling or the Moran process in population genetics, up to a non-universal constant in the noise amplitude depending on the definition of population size and generation time [9, 10, 17–19] that can be absorbed into N. For $\alpha_1 = -\alpha_2 \neq 0$, Eq. (3) resembles the generalized Moran process with weak selection [17]. In various contexts, Eq. (3) and its generalizations have received increasing attention as a simplified model for studying the interplay between selection and genetic drift, e.g. the dilemma of cooperation [20], rare fluctuations in mutualism [21, 22], the crossover from the mean-field behavior to fluctuations-dominated behavior in quantum game theory [23], as well as competition and cooperation in spatial range expansions [14, 17, 24, 25].

Although replicator dynamics with genetic drift is a useful approach, the fixed population size condition has several drawbacks. First, it imposes an artificial growth constraint: the birth of one species necessitates the death of the other even when the two species are neutral variants. Furthermore, population size fluctuations away from a preferred carrying capacity often arise in laboratory experiments, as well as in natural environments. For example, understanding how effectively compressible oceanic flows affect population genetics of marine organisms such as phytoplankton and cyanobacteria [26–29] requires a time-dependent description of local population size, determined by a fluid flow structure. Incorporating spatially dependent population sizes into the evolutionary dynamics of Eq. (3) raises important technical and conceptual challenges [30, 31].

In this paper, with the goal of examining the interplay between number fluctuations, evolutionary and population dynamics in mind, we study a two-species competitive Lotka-Volterra model, one that couples the replicator dynamics to the dynamics of population size. Five deterministic competition and cooperation scenarios similar to replicator dynamics emerge naturally from microscopic birth and competitive death events. Dynamics in finite populations exhibit selection, genetic drift, and growth of population size, as well as population size fluctuations.

We first discuss the limit when long-time dynamics is governed by weak population size fluctuations around a *fixed* stable equilibrium population size. If the two competing species reproduce in the dilute limit at an equal rate, evolutionary and population dynamics approximately decouple near the equilibrium population size. In this case, the effective evolutionary dynamics near the equilibrium population size is described by replicator dynamics with genetic drift. Despite population size fluctuations, Moran model results with and without selection are recovered. Pigolotti *et al.* utilized this limit to extend Eq. (3) to study population genetics in aquatic environments, where population size also varies in both time and space [30].

We then study the limit when evolutionary and population dynamics are coupled and competitions take place with systematically varying population sizes as opposed to fluctuations around a fixed equilibrium population size. We focus on the strong mutualism scenario, where conventional replicator dynamics with genetic drift fails to predict the fixation probability, due to a strong cou-

pling between evolutionary and population dynamics. The problem can be restated as a far from equilibrium escape problem to absorbing boundaries from an attractive fixed point in a two dimensional phase space. The method of matched asymptotic expansions produces *both* the fixation probability and the mean fixation time taking into account the coupled evolutionary and population dynamics .

The paper is organized as follow: Sec. II presents the mean-field and stochastic description of the competitive Lotka-Volterra model. The phase portraits of the model and of the replicator dynamics are compared and contrasted. The emphasis is on parameter values such that an attractive line of approximately fixed population size dominates the long-time dynamics. This limit enables us to identify the mapping between the model and the replicator dynamics. In Sec. III we discuss the limit when the replicator dynamics with genetic drift allows independent population size fluctuations, and show that standard population genetics results for the fixation probability and the mean fixation time in different selection scenarios are recovered. In Sec. IV, we demonstrate the failure of replicator dynamics with genetic drift to describe simulations of strong mutualism with a varying population size. We then construct the fixation probability and the mean fixation time allowing an *arbitrary* initial population size and an initial frequency from the method of matched asymptotic expansions. We conclude with a summary and discussions in Sec. V. Details of analytical calculations are presented in the appendices: Appendix A contains derivations of the coupled stochastic dynamics between the frequency and the population size. Appendix B and Appendix C explain the application of matched asymptotic expansions to achieve the results of Sec. IV.

II. COMPETITIVE LOTKA-VOLTERRA MODEL

The competitive Lotka-Volterra model accounts for natural population growth with limited resources; each individual of the same species S_i undergoes a logistic birth and competitive death process:

$$S_i \xrightarrow{\mu_i} S_i + S_i, \tag{4}$$

$$S_i + S_i \xrightarrow{\lambda_{ii}} S_i, \tag{5}$$

where μ_i is the reproduction rate of species i, and λ_{ii} is the rate of intraspecies competition. The combination of (4), which describes an exponential growth of population in abundant resources, and (5), which dominates when the population size is large, leads to saturation of population size at the carrying capacity $N_i^* = \mu_i/\lambda_{ii}$. Experiments show that a logistic growth model accurately captures the growth dynamics of a single yeast strain in a well-mixed culture [32].

Interspecies interactions are modeled by additional competition

$$S_i + S_j \xrightarrow{\lambda_{ij}} S_j, \tag{6}$$

where λ_{ij} is the rate at which species j wins in the competition for limited resources with species i. In general, $\lambda_{ij} \neq \lambda_{ji}$ for $i \neq j$ although λ_{ij} and λ_{ji} must both be nonnegative in this model. The interaction (6) encapsulates situations when one species suffers from the presence of the others, for example, by secretions of toxins or competition for the same resources. As we will now show, there are 5 generic competition scenarios analogous to replicator dynamics. The population size, however, is not strictly fixed in this more general model, since the reactions (4-6) do not conserve the overall population size.

A. Mean field description

In a well-mixed environment with an infinitely large population size, Eqs. (4)-(6) can be regarded as chemical reactions and determine the mean field dynamics of the number of species i, N_i, as

$$\frac{dN_1}{dt} = (\mu_1 - \lambda_{11}N_1 - \lambda_{12}N_2)N_1, \tag{7}$$

$$\frac{dN_2}{dt} = (\mu_2 - \lambda_{22}N_2 - \lambda_{21}N_1)N_2, \tag{8}$$

where we set the reaction volume to 1. Without interspecies competition, each species i independently grows up and saturates at the carrying capacity $N_i^* = \mu_i/\lambda_{ii}$. Although the carrying capacity of the two species can be different in general, we focus on the case when $N_1^* = N_2^* = N$ for simplicity. By introducing $c_i = N_i/N$, which represents the number of species i relative to its carrying capacity, Eqs. (7) and (8) can be non-dimensionalized to read

$$\frac{1}{(1+s_o)}\frac{dc_1}{d\tilde{t}} = c_1\Big(1 - c_1 - c_2\Big) + \beta_1 c_1 c_2, \tag{9}$$

$$\frac{dc_2}{d\tilde{t}} = c_2\Big(1 - c_1 - c_2\Big) + \beta_2 c_1 c_2, \tag{10}$$

where $\tilde{t}$ is the dimensionless time $\mu_2 t$, s_o is the reproductive advantage of species 1 near the origin defined by $1+s_o \equiv \mu_1/\mu_2$, and the interspecies competitions are absorbed into $\beta_1 \equiv 1-\Big(\frac{\lambda_{12}}{\lambda_{22}}\Big)\Big(\frac{\mu_2}{\mu_1}\Big)$ and $\beta_2 \equiv 1-\Big(\frac{\lambda_{21}}{\lambda_{11}}\Big)\Big(\frac{\mu_1}{\mu_2}\Big)$. Note that the $\{\beta_i\}$ can not exceed unity if $\{\mu_i\}$ and $\{\lambda_{ij}\}$ are positive. Three dimensionless parameters s_o, β_1, β_2 control the phase portraits in the c_1-c_2 plane, which always contain *at least* 3 physically relevant fixed points at $(0,0), (1,0)$, and $(0,1)$, corresponding to the total extinction, the saturation of species 1, and the saturation of species 2, respectively. The fixed point $(0,0)$ is always unstable with the straight heteroclinic trajectories connecting $(0,0)$ to $(1,0)$ and $(0,0)$ to $(0,1)$ describing the

logistic growth of a single species in the absence of the other.

Two dimensionless parameters β_1 and β_2 dictate competition scenarios similar to those described by α_1 and α_2 in the replicator dynamics, provided an initial condition contains non-zero population of both species. However, the overall population size is now allowed to change. These mean field competition scenarios are illustrated in Figs. 2, 3, and 4. If the product $\beta_1\beta_2 < 0$, the species i with positive β_i dominates. The fixed point corresponding to the saturation of the dominating species is stable and the fixed point corresponding to the saturation of the extinct species is a saddle point.

When $\beta_1\beta_2 > 0$, a fourth dynamically relevant fixed point appears at $\boldsymbol{c}^* = \frac{1}{\beta_1+\beta_2-\beta_1\beta_2}(\beta_1, \beta_2)$. If both β_1 and β_2 are negative, we have a bistable situation similar to *antagonism.* Initial conditions that lie on the basin of attraction of the fixed point $(1, 0)$ and $(0, 1)$ result in the total domination (i.e., fixation) of species 1 and species 2, respectively. The coexistence fixed point $\boldsymbol{c}^*$ is a saddle point whose stable 1-d manifold consists of the separatrices such as the trajectory connecting $(0, 0)$ to $\boldsymbol{c}^*$. Here, coexistence is fragile and only possible for initial conditions lying exactly on these separatrices.

When both β_1 and β_2 are positive, stable coexistence emerges at the stable fixed point $\boldsymbol{c}^*$ similar to *mutualism.* Although we shall refer to this scenario as mutualism to conform to Refs. [14] and [30], we emphasize that interspecies interactions actually arise from underlying competitive interactions. In our case, interspecies interactions reduce the growth rate per capita of both species and restrict $\lambda_{ij} > 0$ or equivalently $\beta_i < 1$. Stable coexistence can persist despite the competition. The population size at $\boldsymbol{c}^*$, however, reduces to $\frac{\beta_1+\beta_2}{\beta_1+\beta_2-\beta_1\beta_2}N$ relative to the upper bound $2N$ attained in the absence of interspecies competition ($\lambda_{12} = \lambda_{21} = 0$, or equivalently $\beta_1 = \beta_2 = 1$.)

Lastly, the exceptional case $\beta_1 = \beta_2 = 0$ resembles neutral evolution such that every point on a one dimensional line $c_1 + c_2 = 1$ is a fixed point. We shall call this fixed line scenario *quasi-neutral evolution* as the two species will not be neutral variants in the dilute limit if $s_o \neq 0$: A reproductive advantage near the origin does not destroy the coexistence line $c_1 + c_2 = 1$, but instead modifies the relative abundance of the two species as population size grows and saturates somewhere on the fixed line $c_1 + c_2 = 1$. The next subsection discusses the approach toward population size saturation.

B. Growth of population size and mapping to deterministic replicator dynamics when $|\beta_i| \ll 1$

Despite the rough similarity of the scenarios above to those of replicator dynamics, the competitive Lotka-Volterra model contains the overall population size as a dynamical variable. In general, growth and competition together do not conserve the population size, as illustrated in Fig. 4. In the limit $|\beta_1| \ll 1$ and $|\beta_2| \ll 1$, however, there is an attractive 1-d manifold of approximately fixed population size $c_1+c_2 \approx 1$ on which conventional replicator dynamics determines the ultimate outcome. We shall refer to the competition near the line $c_1 + c_2 = 1$ in this limit as the competition under the *replicator condition.* Under the replicator condition, the balance between growth and competitive death

results in an effective replicator dynamics with an approximately fixed population size, which we discuss below. Figs. 2 and 3 illustrate competitions in this limit.

We now discuss the growth of population size toward the replicator condition and the eventual mapping onto the replicator dynamics. Upon using $c_T \equiv c_1+c_2$ to measure the overall population size and defining $f \equiv c_1/c_T$ as the frequency of species 1, we obtain the following coupled dynamics of c_T and f from Eq. (7) and Eq. (8),

$$\frac{dc_T}{d\tilde{t}} = (1 + s_o f)v_G(c_T) + (\alpha_1 + \alpha_2)f(1 - f)c_T^2, \quad (11)$$

$$\frac{df}{d\tilde{t}} = v_E(f) + s_o f(1 - f)(1 - c_T), \quad (12)$$

where the function $v_G(c_T) \equiv c_T(1 - c_T)$ in Eq. (11) describes the logistic growth of population size, and the evolutionary dynamics term in Eq. (12) $v_E(f) \equiv [\alpha_1 + (\alpha_1 + \alpha_2)f]f(1 - f)$ resembles the frequency-dependent selection in Eq. (2) with the identification

$$\alpha_1 = (1 + s_o)\beta_1, \quad \text{and} \quad \alpha_2 = \beta_2. \quad (13)$$

We first analyze the quasi-neutral evolution scenario when $\beta_1 = \beta_2 = 0$, and then treat the case $0 < |\beta_i| \ll 1$ as a weak perturbation. In the quasi-neutral scenario, $\alpha_1 + \alpha_2 = 0$ and c_T obeys $\frac{dc_T}{d\tilde{t}} = (1 + s_o f)v_G(c_T)$. For any non-zero initial population size, c_T eventually saturates at $c_T = 1$, which is an attractive 1-d manifold of fixed points in the original (c_1, c_2) phase space. As the population size grows from $c_T(0) < 1$ or declines from $c_T(0) > 1$ to saturate at $c_T = 1$, $c_1(t)$ and $c_2(t)$ change to conserve the variable ρ defined by

$$\begin{aligned} \rho &\equiv c_2(t)/c_1(t)^{1/(1+s_o)}, \\ &= c_2(0)/c_1(0)^{1/(1+s_o)}, \end{aligned} \quad (14)$$

because Eq. (9) and Eq. (10) with $\beta_1 = \beta_2 = 0$ implies $d\rho/d\tilde{t} = 0$. To see how the frequency of each species changes as the population size approaches $c_T = 1$, it's helpful to rewrite ρ in terms of f and c_T as

$$\rho = c_T(t)^{s_o/(1+s_o)}[1 - f(t)]/f(t)^{1/(1+s_o)}. \quad (15)$$

Since ρ is a conserved variable, Eq. (15) implies that the frequency of a reproductively advantageous species increases as $c_T(t)$ grows toward $c_T = 1$ when $c_T(0) \ll 1$. On the other hand, the frequency of a reproductively advantageous species decreases as $c_T(t)$ declines toward $c_T = 1$ when $c_T(0) \gg 1$. If both species grow up at an equal rate ($s_o = 0$), the frequency of each is independently conserved, regardless of $c_T(t)$.

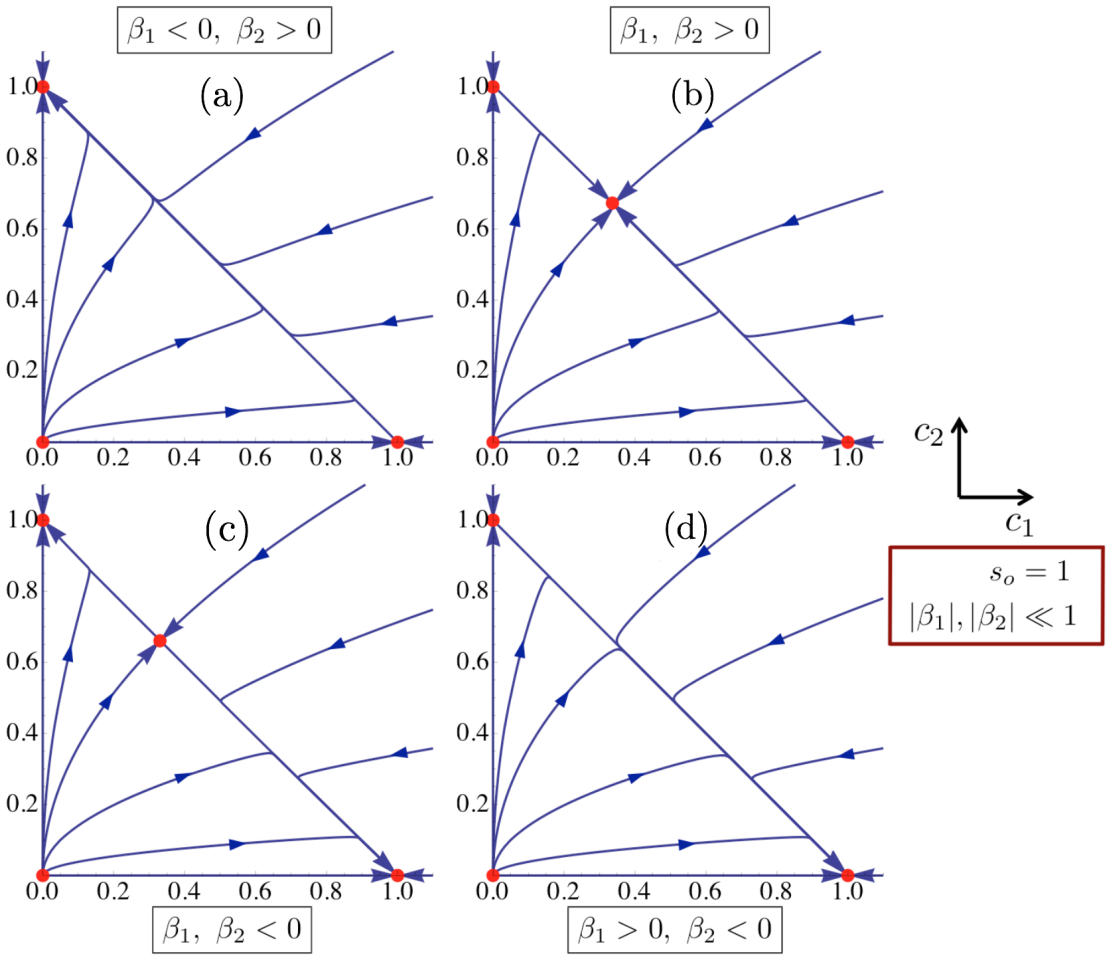

FIG. 2. (Color online) The phase portraits of competitive Lotka-Volterra dynamics with $s_o = 1$, $|\beta_2| = 0.028$ and $|\beta_1| = 0.014$ in the (c_1, c_2)-plane. The competition scenario depends on the sign of β_1 and β_2, similar to α_1 and α_2 in Fig. 1. Cases (a),(b),(c), and (d) correspond to species 2-domination, mutualism, antagonism, and species 1-domination, respectively. Red circles represent fixed points and blue lines correspond to mean field trajectories of Eqs. (9) and (10) solved numerically. For $s_o = 1$, population size relaxes toward the replicator condition ($c_T \approx 1$) along a curved trajectory of constant ρ, which forms an upper branch of the parabola $c_1 = \rho^2 c_2^2$. Deviation from a trajectory of fixed ρ only becomes apparent close to the line $c_T = 1$. Once the replicator line $c_1 + c_2 \approx 1$ is reached, the replicator dynamics at a fixed population size takes over.

For $0 < |\beta_1| \ll 1$ and $0 < |\beta_2| \ll 1$, the dynamics of population size away from $c_T = 1$ still obeys $\frac{dc_T}{d\tilde{t}} \approx (1 + s_o f) v_G(c_T)$ since $(1 + s_o f) v_G(c_T) \gg [\alpha_1 + \alpha_2] f(1-f) c_T^2$ in Eq. (11). Moreover, the approach toward $c_T = 1$ again follows a trajectory of approximately constant ρ since, away from $c_T = 1$,

$$\begin{aligned}\left|\frac{d}{d\tilde{t}} \ln \rho\right| &= \left|c_T[(\beta_2 - \beta_1) + (\beta_2 + \beta_1) f]\right| \\ &\ll \Big|(1 + s_o f)(1 - c_T) \\ &\quad + [(1 + s_o)\beta_1 + \beta_2] f(1-f) c_T\Big| \\ &= \left|\frac{d}{d\tilde{t}} \ln c_T\right|.\end{aligned}$$

Once c_T is in close proximity to 1, ρ is no longer approximately conserved. The thin neighborhood of $c_T = 1$ in which conservation is strongly violated, however, becomes vanishingly small in the limit $|\beta_i| \ll 1$. Accordingly, we can set $c_T = 1$ in Eq. (11) and Eq. (12) to find in this neighborhood

$$\frac{dc_T}{d\tilde{t}} \approx 0 \quad \text{and} \quad \frac{df}{d\tilde{t}} = v_E(f), \tag{16}$$

which reproduces deterministic replicator dynamics of a fixed population size N. The mean field trajectories in Figs. 2 and 3 depict the approach toward the replicator condition in which the replicator dynamics at $c_T = 1$ determines how the frequency of each species changes. Fig. 2 illustrates growth along the bent trajectories $c_1(t) = \rho^2 c_2(t)^2$ that arises when species 1 has a repro-

ductive advantage near the origin ($s_o = 1$), while Fig. 3 depicts growth along a set of straight lines of fixed species' frequency when $s_o = 0$.

C. Stochastic dynamics

In finite populations, the ultimate fate of the coupled system depends not only on the 3 dimensionless parameters s_o, β_1, β_2 and the initial condition, but also on fluctuation corrections to the mean-field dynamics due to microscopic stochasticity. We can quantify the stochastic dynamics by regarding the microscopic rates in Eqs. (4)-(6) as Markov processes. The joint probability distribution of finding N_i individuals of species i at time t, $P(N_1, N_2, t)$, then obeys the Master equation

$$\begin{aligned}\partial_t P(N_1,N_2,t) =& \mu_1(N_1-1)P(N_1-1,N_2,t)\\ &+\mu_2(N_2-1)P(N_1,N_2-1,t)\\ &+\lambda_{11}N_1(N_1+1)P(N_1+1,N_2,t)\\ &+\lambda_{22}N_2(N_2+1)P(N_1,N_2+1,t)\\ &+\lambda_{12}N_2(N_1+1)P(N_1+1,N_2,t)\\ &+\lambda_{21}N_1(N_2+1)P(N_1,N_2+1,t)\\ &-\Big[\,\mu_1N_1+\mu_2N_2\\ &\quad+\lambda_{11}N_1(N_1-1)+\lambda_{22}N_2(N_2-1)\\ &\quad+\lambda_{12}N_1N_2+\lambda_{21}N_1N_2\,\Big]P(N_1,N_2,t).\end{aligned}$$

In the limit $1/N \ll 1$ (recall that $N = \mu_1/\lambda_{11} = \mu_2/\lambda_{22}$), this discrete Master equation can be approximated by the Fokker-Planck equation for the continuous probability distribution $P(c_1, c_2, t)$ via the Kramers-Moyal expansions or the Van-Kampen $1/N$ expansions [33, 34]. The corresponding Fokker-Planck equation for the probability $P(\boldsymbol{c}, t)$ of a particular species configuration $\boldsymbol{c}$ reads

$$\partial_t P(\boldsymbol{c},t) = \sum_{i=1}^{2}\Big(-\partial_{c_i}[v_i(\boldsymbol{c})P(\boldsymbol{c},t)] + \frac{1}{2N}\partial^2_{c_i}[D_i(\boldsymbol{c})P(\boldsymbol{c},t)]\Big), \qquad (17)$$

where the deterministic drift and N-independent diffusion coefficients are

$$v_1(\boldsymbol{c}) = \mu_1 c_1(1-c_1-c_2) + \mu_1\beta_1 c_1 c_2, \qquad (18)$$
$$v_2(\boldsymbol{c}) = \mu_2 c_2(1-c_1-c_2) + \mu_2\beta_2 c_1 c_2, \qquad (19)$$
$$D_1(\boldsymbol{c}) = \mu_1 c_1(1+c_1+c_2) - \mu_1\beta_1 c_1 c_2, \qquad (20)$$
$$D_2(\boldsymbol{c}) = \mu_2 c_2(1+c_1+c_2) - \mu_2\beta_2 c_1 c_2. \qquad (21)$$

An equivalent representation in terms of the Ito calculus [34] prescribes stochastic dynamics of the $c_i(t)$ that resembles a set of coupled Langevin equations:

$$\frac{dc_i}{dt} = v_i(\boldsymbol{c}) + \sqrt{\frac{D_i(\boldsymbol{c})}{N}}\Gamma_i(t), \qquad (22)$$

where $\Gamma_i(t)$ is a Gaussian white-noise with $\langle\Gamma_i(t)\Gamma_j(t')\rangle = \delta_{i,j}\delta(t-t')$ and $\langle\Gamma_i(t)\rangle = 0$. In the limit of infinitely large population size N, the noise term of order $\sqrt{1/N}$ in Eq. (22) vanishes and we recover the mean-field description of Eq. (9) and Eq. (10). Note that the deterministic drift can not be written as a gradient of a potential function since $|\nabla\times\vec{v}(\boldsymbol{c})| \equiv |\partial_1 v_2(\boldsymbol{c}) - \partial_2 v_1(\boldsymbol{c})| = |\mu_1(1-\beta_1)c_1 - \mu_2(1-\beta_2)c_2| \neq 0$. In contrast to diffusion in a potential field, the non-potential drift is typical for stochastic non-linear dynamics in a higher dimensional phase space [34, 35]. Hence, standard tools for analyzing the statistics of fluctuations such as eigenfunction expansions of the Fokker-Planck equation [36] or saddle-point approximations of the most probable escape path [33, 37] are not directly applicable.

For finite N, number fluctuations alter the mean-field description and can lead to outcomes different from the deterministic predictions. For instance, fluctuations will eventually drive one of the two species to fixation and destroy stable coexistence for mutualism. Regardless of the deterministic phase portraits, the eventual fate of the system at long times is fixation of a single species. Once one species becomes fixed, the dynamics of the fixed species follow stochastic logistic growth while the other species remains forever extinct, as is easily checked from Eqs. (18)-(22). The c_1 and c_2 axes are thus *absorbing boundaries* leading to the fixation of species 1 and of species 2, respectively. The only absorbing state in the phase space is total extinction (0,0), which is inaccessible since we don't allow for the death process $S_i \to \phi$ in our simulations. Had we included the death process, the total extinction would nevertheless be extremely unlikely because the mean time to extinction for logistic growth grows exponentially with N [38].

If time is non-dimensionalized to $\tilde{t} = \mu_2 t$ in Eqs. (18)-(22), the stochastic dynamics then depends on only 4 dimensionless parameters: s_o, β_1, β_2, and $1/N$. The parameters s_o, β_1, β_2 control both the mean-field phase portrait and the diffusion coefficients, while the parameter $1/N$ sets the strength of fluctuations relative to deterministic drift.

In the following sections, we investigate the dynamics in different ranges of s_o, β_1, β_2 assuming small fluctuations, $1/N \ll 1$. In Sec. III, we study the limit when $|\beta_i| \ll 1$ with typical stochastic trajectories shown in Fig. 3 for $s_o = 0$. In Sec. IV, we highlight the limitations of fixed population size replicator dynamics by studying a strong mutualism scenario where β_1 and β_2 are $\mathcal{O}(1)$ and we set $s_o = 0$ for simplicity. Fig. 4 illustrates the stochastic dynamics in this case, where the time dependence of the overall population size plays a crucial role. In this situation, replicator dynamics is *never* an appropriate description.

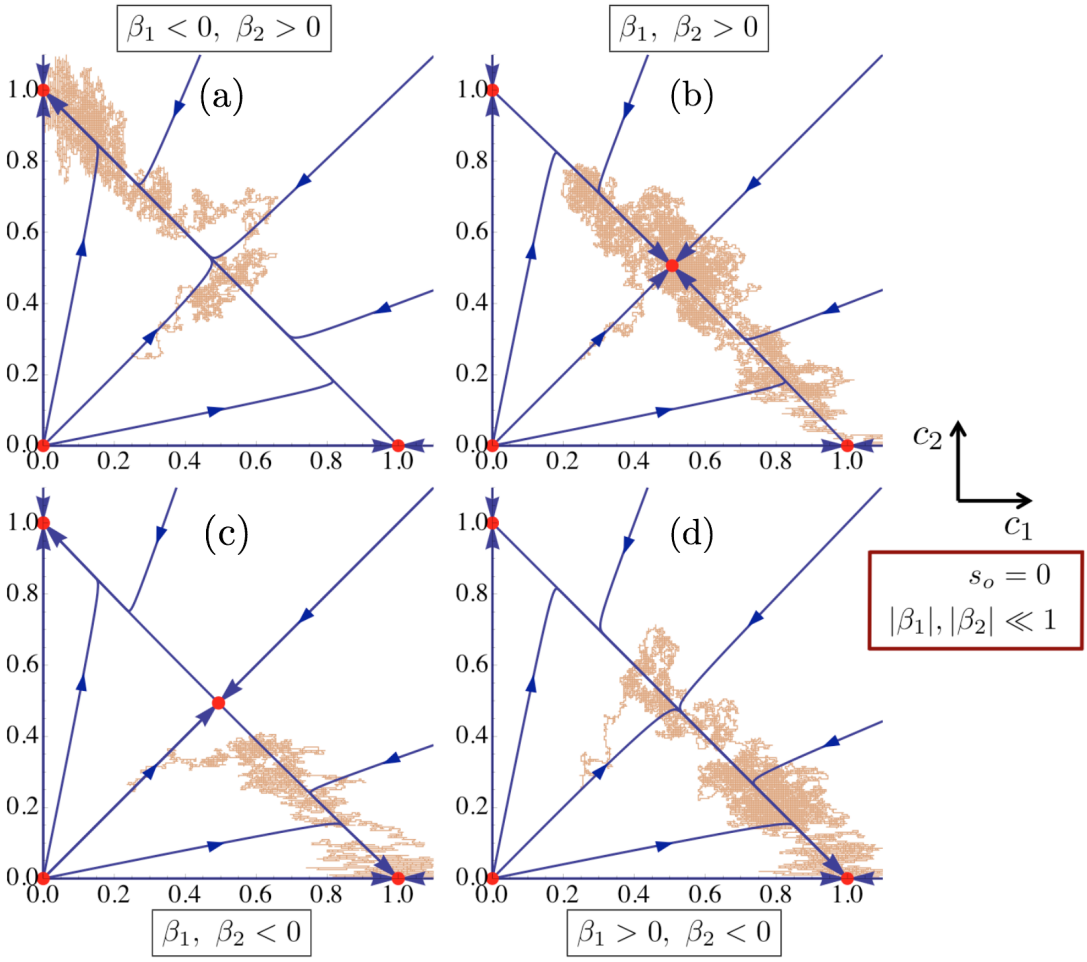

FIG. 3. (Color online) Replicator dynamics with genetic drift and population size fluctuations when $c_T \approx 1$. Cases (a),(b),(c), and (d) again correspond to species 2-domination, mutualism, antagonism, and species 1-domination, respectively with $s_o = 0$, and $|\beta_1| = |\beta_2| = 0.03$. In this case, the mean field trajectories approach the replicator condition ($c_1 + c_2 = c_T \approx 1$) as straight lines that preserve the initial species frequency f. Each orange stochastic trajectory, simulated from the Gillespie's algorithm with the initial condition $(f, c_T) = (0.5, 0.5)$ (i.e., $c_1 = c_2 = 0.25$) and $N = 100$ individuals, demonstrates a typical fixation event. Stochastic trajectories show rapid growth of population size toward the replicator condition where selection, genetic drift, and population size fluctuations ultimately determine the competition outcome.

III. REPLICATOR DYNAMICS WITH GENETIC DRIFT AND POPULATION SIZE FLUCTUATIONS

We now follow Pigolotti *et al.* [30] and discuss competitive Lotka-Volterra dynamics under the replicator condition ($c_T \approx 1$ and $|\beta_i| \ll 1$) and $1/N \ll 1$, thus extending Eq. (3) to include fluctuations in the overall population size. We recast earlier results of Ref. [30] in the language of conventional replicator dynamics with genetic drift, to better illustrate the breakdown of this approach for the case of strong mutualism discussed in Sec. IV. Our focus is on the dynamics of $f(t)$, the frequency of species 1, and the total population size $c_T(t)$. When $s_o = 0$ and $|\beta_i| \ll 1$, (Appendix A also treats $s_0 \neq 0$ a case not considered in Ref. [30]) Appendix A shows that the coupled stochastic dynamics of f and c_T for $c_T \approx 1$ read [30]

$$\frac{df}{dt} = \mu v_E(f) c_T + \sqrt{\frac{\mu D_g(f)}{N}\left(\frac{1+c_T}{c_T}\right)}\Gamma_f(t), \quad (23)$$

$$\frac{dc_T}{dt} = \mu v_G(c_T) + \sqrt{\frac{\mu c_T(1+c_T)}{N}}\Gamma_{c_T}(t), \quad (24)$$

where $\Gamma_i(t)$ is an uncorrelated Gaussian white noise with zero mean and unit variance, $D_g(f) = f(1-f)$ is the frequency-dependent genetic drift coefficient [10, 11], $v_E(f)$ and $v_G(c_T)$ are the selection function and the logistic growth function that appear in Eqs. (11) and (12). These stochastic differential equations, which arise from a more general dynamics with $s_o \neq 0$ discussed in Ap-

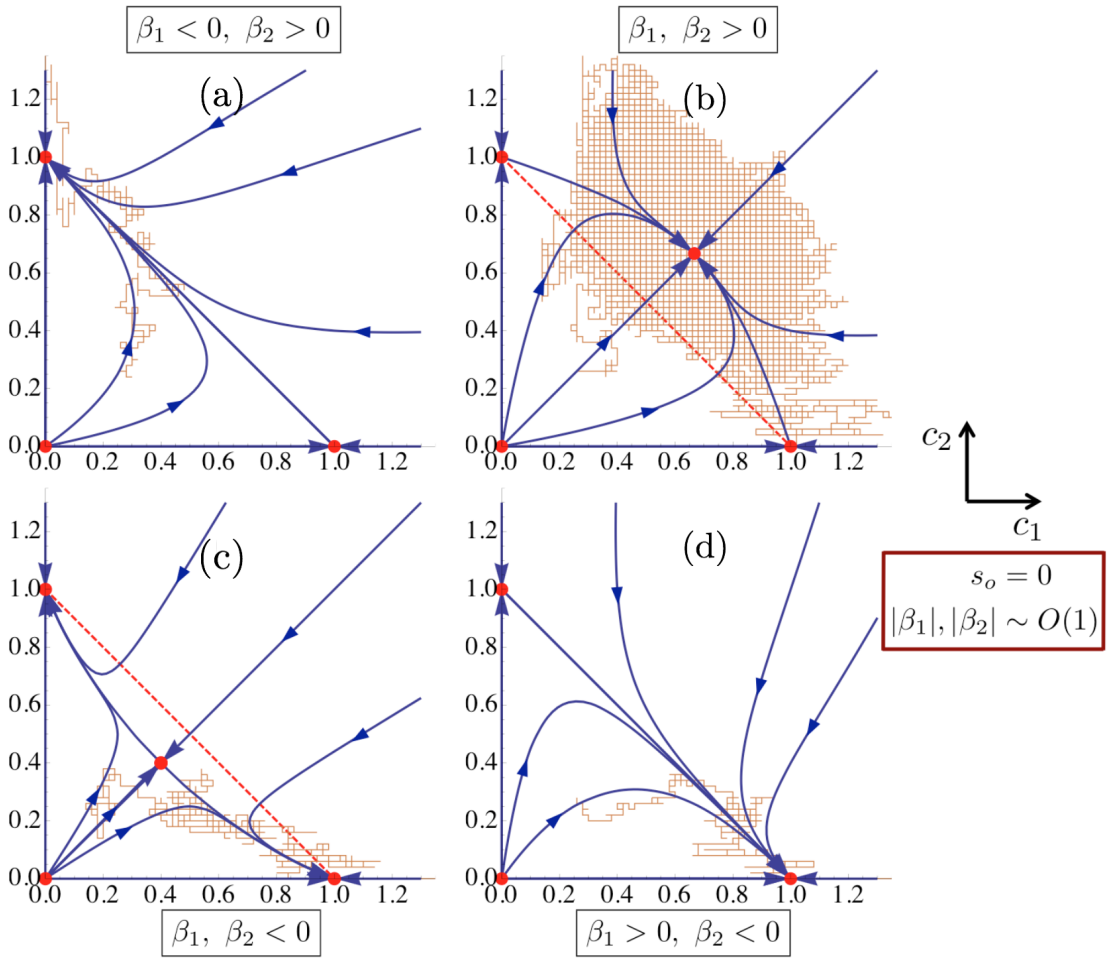

FIG. 4. (Color online) The phase portraits for $s_o = 0$, and $|\beta_1| = |\beta_2| = 0.5$, which includes the case of strong mutualism of Sec. IV. Competition at long times no longer takes place close to the line $c_1 + c_2 = c_T = 1$, depicted as the red dashed line in (b) and (c), but with a varying overall population size. Cases (a),(b),(c), and (d) correspond to species 2-domination, mutualism, antagonism, and species 1-domination, respectively. The initial condition for the stochastic simulation is $(f, c_T) = (0.5, 0.5)$ (i.e., $c_1 = c_2 = 0.25$) with $N = 50$ individuals. In contrast to mutualism under the replicator condition (e.g., Fig. 3(b) with $|\beta_1|, |\beta_2| \ll 1$), the coexistence fixed point in strong mutualism shown in (b) is highly stable and fixation becomes a rare event even when N is as small as 50.

pendix A, must be interpreted in terms of Ito calculus [33, 34] in order to correctly reproduce the Fokker-Planck Equation (17). We have retained the original unit of time to make the reproduction time scale explicit and denoted $\mu = \mu_2$ for brevity.

In Eq. (24), the dynamics of population size is f-independent and exhibits a combination of fast approximately deterministic relaxation toward the equilibrium line $c_T = 1$ and slow fluctuations with variance $1/N$ around this equilibrium. On the other hand, the dynamics of f depends on c_T. Nevertheless, it is mostly influenced by the mean population size $\langle c_T \rangle = 1$ since the variance of c_T about $c_T = 1$ is $1/N \ll 1$. Thus, the effective dynamics of f, accurate to first order in $1/N$, can be approximated by simply replacing $c_T = 1$, which leads to

$$\frac{df}{dt} = \mu v_E(f) + \sqrt{\frac{2\mu}{N} D_g(f)} \Gamma_f(t). \tag{25}$$

Eq. (24) and Eq. (25) together describe the dynamics near the replicator condition when $1/N \ll 1$, which is precisely Eq. (3), with the addition of an independently fluctuating population size around the fixed mean $c_T = 1$.

Note that the variance per generation time of Eq. (25) given by $f(1-f)/N$ is independent of both the population size fluctuations away from $c_T = 1$ and the selection mechanism in the vicinity of this line. In fact, the variance resembles that of the Wright-Fisher or Moran model [10]. Thus, the effective population size deduced from the variance of the genetic drift is equivalent to the

mean population size N despite fluctuations in the overall population size.

From the closed form Eq. (25) for $f(t)$, we can recover known results for the fixation probability $u(f)$ and the mean fixation time $\tau(f)$ which are, respectively, the probability that species 1 become fixed (instead of species 2) and the average time to lose heterozygosity provided species 1 initially has a frequency f at $c_T = 1$. These quantities obey ordinary differential equations,

$$v_E(f)\frac{d}{df}u(f) + \frac{D_g(f)}{N}\frac{d^2}{df^2}u(f) = 0, \tag{26}$$

$$v_E(f)\frac{d}{df}\tau(f) + \frac{D_g(f)}{N}\frac{d^2}{df^2}\tau(f) = -\frac{1}{\mu}, \tag{27}$$

subject to the boundary conditions $u(0) = 0, u(1) = 1$ and $\tau(0) = \tau(1) = 0$ [33, 34]. The differential equations can be integrated directly leading to closed form solutions which read

$$u(f) = \frac{\int_0^f e^{-N\Psi(x)}\,dx}{\int_0^1 e^{-N\Psi(x)}\,dx}, \tag{28}$$

where $\Psi(x) \equiv \int_0^x v_E(y)/D_g(y)\,dy$, and

$$\tau(f) = I(1)u(f) - I(f), \tag{29}$$

where $I(f) \equiv [\int_0^f dx\, e^{-N\Psi(x)} \int_1^x dy\, e^{N\Psi(y)}/D_g(y)](N/\mu)$.

We now review the implications of Eq. (25) for different selection scenarios. In neutral evolution ($\beta_1 = \beta_2 = 0$), Eq. (25) becomes (with $D_g(f) = f(1-f)$)

$$\frac{df}{dt} = \sqrt{\frac{2\mu}{N}D_g(f)}\Gamma_f(t), \tag{30}$$

which is a continuous approximation of the Moran model or the Wright-Fisher sampling in population genetics [9–11, 39, 40]. Only genetic drift participates in the dynamics and fixation events are results of an unbiased random walk with $c_T \approx 1$ toward $f = 0$ or $f = 1$, absorbing boundaries, and independent fluctuations of population size about the mean N. In this case, direct evaluation of Eqs. (28) and (29) gives [39]

$$u_{neutral}(f) = f, \tag{31}$$

$$\tau_{neutral}(f) = -\left(\frac{N}{\mu}\right)\Big[f\ln f + (1-f)\ln(1-f)\Big], \tag{32}$$

where f is the initial frequency of species 1.

For selection that favors domination of one species, the special case $\tilde{s} \equiv \beta_1 = -\beta_2$ reproduces the Moran process with an effective selective advantage $\tilde{s}$ (provided $c_T \approx 1$), described by

$$\frac{df}{dt} = \mu\tilde{s}f(1-f) + \sqrt{\frac{2\mu}{N}D_g(f)}\Gamma_f(t). \tag{33}$$

We emphasize that the growth rates of the two species when $c_T \ll 1$ in this particular competitive Lotka-Volterra dynamics are strictly identical ($s_o = 0$), but the species with positive β_i nevertheless behaves near $c_T = 1$ as if it has a selective advantage $\tilde{s}$. Upon evaluating Eq. (28), we arrive at the celebrated Kimura result for the fixation probability [18]

$$u(f) = \frac{1 - e^{-\tilde{s}Nf}}{1 - e^{-\tilde{s}N}}. \tag{34}$$

A lengthy closed-form formula for the mean fixation time can also be obtained; see for example Ref. [20].

For antagonistic or mutualistic interactions, the effective dynamics of f reads

$$\frac{df}{dt} = \mu\tilde{\beta}f(1-f)(f^* - f) + \sqrt{\frac{2\mu}{N}D_g(f)}\Gamma_f(t), \tag{35}$$

where $f^* = \beta_1/(\beta_1 + \beta_2)$ is the coexistence fixed point with $c_T \approx 1$ and $\tilde{\beta} \equiv (\beta_1 + \beta_2)$ controls the stability of f^*. The parameter $\tilde{\beta}$ is positive and negative for mutualism and antagonism, respectively. In either case, the fixation probability directly follows from Eq. (28), and is given by

$$u(f) = \frac{\int_0^f e^{\frac{N\tilde{\beta}}{2}(f^*-f)^2}df}{\int_0^1 e^{\frac{N\tilde{\beta}}{2}(f^*-f)^2}df}, \tag{36}$$

in agreement with Ref. [14]. It appears that the mean fixation time from Eq. (29) can not be simplified further, and must be evaluated numerically.

Pigolotti *et al.* simulated the fixation probability for different competition scenarios under the replicator condition with $s_o = 0$ and found good agreement with these predictions of the fixation probabilities even for fairly small population sizes of $O(N) \sim 100$ individuals [30]. Constable *et al.* also studied this limit using a different mathematical technique and found good agreement between theories and simulations of both the fixation probability and the mean fixation time [41]. These results confirm that the competitive Lotka-Volterra model reduces to replicator dynamics with genetic drift and an independently fluctuating overall population size, *provided* $s_o = 0$, $|\beta_i| \ll 1$, and $c_T \approx 1$.

We mention briefly that when $s_0 \neq 0$, the long-time dynamics still fluctuates around the equilibrium line $c_T = 1$ provided $|\beta_i| \ll 1$; however, evolutionary dynamics now couples to population dynamics, see Appendix A. An interesting phenomenon of fluctuation-induced selection arises as a result of this coupling near the equilibrium line. In the scenario of quasi-neutral evolution ($\beta_1 = \beta_2 = 0$), species with a *reproductive disadvantage* in the dilute limit acquires a *selective advantage* for competitions near the equilibrium line [42–45]. The resulting effective evolutionary dynamics near the equilibrium line contains not only a fluctuation-induced selective advantage, but also an unusual genetic drift of a non-Wright-Fisher (and non-Moran) type [42–45].

IV. STRONG MUTUALISM WITH A VARYING POPULATION SIZE

In this section, we study a strong mutualism scenario ($\beta_i \sim \mathcal{O}(1)$ in Fig. 4(b)), where the replicator condition is no longer satisfied. In this limit, the coexistence fixed point shifts far away from the line $c_T = 1$ and becomes strongly attractive in all eigen-directions. The faint orange grid in Fig. 4(b) illustrates a typical fixation trajectory exhibiting a decline of overall population size as weak fluctuations about the strongly stable fixed point eventually drive one of the two species (in this case, species 1) to fixation.

A. Failure of the fixed population size model near boundary layers

Suppose we accept Eq. (3) as a phenomenological model for mutualism and fit the resulting fixation probability in Eq. (36) to simulation data; how well would this model with a strictly fixed population size do? To motivate the choice of fitting parameters, we first discuss the behavior of the fixation probability $u(f)$ predicted by Eq. (36). For $\tilde{\beta}N \ll 1$ (recall that $\tilde{\beta} \equiv \beta_1 + \beta_2$ in Eq. (36)), genetic drift dominates mutualistic selection and the fixation probability approaches the result of an unbiased random walk of neutral evolution, Eq. (31). For $\tilde{\beta}N \gg 1$, the coexistence fixed point is metastable and fixation driven by weak genetic drift becomes a rare event. Initial conditions in close proximity to f^* almost surely visit f^* before fixation occurs, giving rise to a plateau of equal fixation probability $u(f^*)$ in the neighborhood of f^*. Furthermore, the fixation probability $u(f)$ only varies rapidly within the boundary layers of width $\sim 1/N$ adjacent to each of the absorbing states $f = 0$ and $f = 1$, away from which $u(f)$ exhibits crossovers to a plateau value $u(f^*)$. The boundary layers near the absorbing states contain initial conditions that can be driven by genetic drift to fixation before being attracted toward f^*. For symmetric mutualism ($f^* = 1/2$), the plateau height $u(f^*)$ is $1/2$ by symmetry from Eq. (36) and is independent of N. For asymmetric mutualism, the N-dependent behavior of $u(f^*)$ can be understood by studying rare event escape from a metastable state. For an evolutionary game with a stable coexistence fixed point, it can be shown that $u(f^*)$ is given by the ratio of the flux into the absorbing state $f = 1$ to the total flux into the absorbing states $f = 0$ and $f = 1$ whose N-dependent behavior in the limit $N \gg 1$ is given by [21, 22]

$$u(f^*) \approx \frac{1}{1 + e^{-N\Delta S_0 + \Delta S_1}}, \tag{37}$$

where, from the perspective of a Feynman's path integral formulation of stochastic dynamics [46, 47], $\Delta S_0 \equiv S_0[\gamma_{f^*\to 1}] - S_0[\gamma_{f^*\to 0}]$ is the difference between the "action" $S_0[\gamma_{f^*\to x}]$ associated with the most probable escape path $\gamma_{f^*\to x}$ beginning at f^* and ending at an absorbing state x, and $\Delta S_1 \equiv \ln w[\gamma_{f^*\to 1}] - \ln w[\gamma_{f^*\to 0}]$ is the difference between fluctuations corrections to the action of the most probable escape path. The N-independent functions ΔS_0 and ΔS_1 are known analytically [21, 22] but are unnecessary for illustrating the failure of the fixed population size model. Note that Eq. (37) resembles the Boltzmann weight in equilibrium statistical mechanics if N is interpreted as inverse temperature while $S_0[\gamma_{f^*\to x}]$ and $\ln w[\gamma_{f^*\to 0}]$ play the role of energy and entropy, respectively, as in the classical Kramers escape-over-a-barrier problem due to thermal fluctuations [36]. For $f^* > 1/2$, it is more likely for species 1 to be fixed and we can infer from Eq. (37) that $\Delta S_0 > 0$, resulting in $u(f^*) \to 1$ as $N \to \infty$. Similar arguments give $\Delta S_0 < 0$ if $f^* < 1/2$, implying that $u(f^*) \to 0$ as $N \to \infty$.

We now denote the two free parameters of Eq. (36) by $\tilde{\beta}N_{eff}$ and f^*_{eff} , and fit $u(f)$ to our numerically simulated fixation probability for strong asymmetric mutualism with $s_o = 0,\ \beta_1 = 0.75,$ and $\beta_2 = 0.70$ whose actual coexistence fixed point is $(f^*, c^*_T) \approx (0.517, 1.568)$. Our stochastic simulations employ the Gillespie algorithm to efficiently simulate the discrete Master equation of Sec. II C [48, 49]. The simulated fixation probabilities for each initial condition are constructed from 10^4 realizations of fixation events. The initial overall population size in our simulations is taken to be $c_T = 1 < c^*_T$, i.e., the initial overall population size is less than the fixed point value. The simulated results shown in Fig. 5 reveal a plateau of equal fixation probability even for relatively small $N \gtrsim 12$. To match the center of the plateau, we choose $f^*_{eff} = f^*$. The other free parameter $\tilde{\beta}N_{eff}$ controls both the plateau height and width. Because the plateau structure occupies most region, it is reasonable to adjust $\tilde{\beta}N_{eff}$ so that $u(f^*)$ matches the height of the simulated plateau. With this fitting procedure, the plateau in the fixed population size model is guaranteed to agree with the simulated plateau.

Although the fixed population size model can be adjusted to fit the elongated plateau in agreement with simulations, it fails to capture the behavior near the absorbing boundaries as revealed by Fig. 5, where the simulated points systematically fall away from the predicted dashed lines. In fact, it is precisely this boundary behavior that distinguishes the fixation probability of mutualism with a fixed population size from mutualism with a varying population size. As we now show, the elongated plateaus also exist for strong mutualism with a varying population size, but the behavior near absorbing boundaries depends on the delicate interplay between the relative frequency and the overall population size.

B. The fixation probability and the mean fixation time from matched asymptotic expansions

We now study the fixation probability and the mean fixation time, taking into account *both* the frequency and

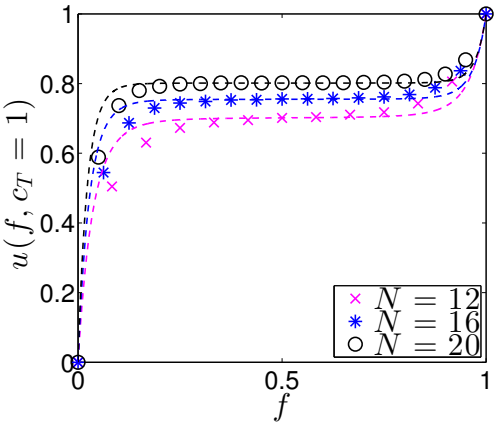

FIG. 5. (Color online) Comparison between fixed population size predictions given by Eq. (36) (dashed lines) and the simulated fixation probabilities from the Gillespie's algorithm (symbols) for an asymmetric strong mutualism with a varying population size with $s_o = 0$, $\beta_1 = 0.75$, and $\beta_2 = 0.70$. The plateau-fitting procedure yields the fitting parameters $f^*_{eff} = f^* = \beta_1/(\beta_1 + \beta_2) \approx 0.517$ and $\tilde{\beta} N_{eff} = 58.0,\ 74.4,\ 91.0$ for the simulated $N = 12,\ 16,\ 20$, respectively. This procedure always fits the plateau, but fails to capture the boundary layer behavior.

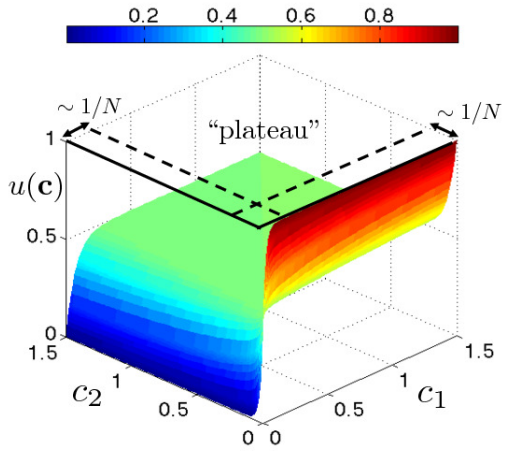

FIG. 6. (Color online) The fixation probability for strong symmetric mutualism with vanishing reproductive advantage near the origin ($s_o = 0$), $\beta_1 = \beta_2 = 0.75$ and $N = 20$ from the matched asymptotic expansions. In the boundary layers adjacent to the absorbing boundaries, the fixation probability shows crossovers with the characteristic width $1/N$ from the boundary condition values to the plateau value $P = 1/2$. Within the boundary layers, fixation at early times before approaching the vicinity of the coexistence fixed point is likely. In contrast, initial conditions in the plateau almost surely arrive at the coexistence fixed point before rare fluctuations eventually leads to fixation. The heat map provides an alternative representation of $u(\boldsymbol{c})$.

the population size degrees of freedom. Our results for the fixation probability are summarized in Fig. 6. A fixation event with initial frequency f and initial population size c_T requires a two-dimensional escape to an absorbing boundary from the initial condition which we specify as $(fc_T, (1-f)c_T)$ in the (c_1, c_2) coordinates. In contrast to mutualism under the replicator condition ($0 < \beta_i \ll 1$ and $c_T \approx 1$), there is no dimensional reduction to an effectively one-dimensional dynamics with approximately fixed $c_T \approx 1$ here. In fact, the fixation probability $u(\boldsymbol{c})$ obeys a two-dimensional backward Kolmogorov equation, namely

$$0 = \sum_{i=1}^{2} \Big(v_i(\boldsymbol{c}) \partial_{c_i} u(\boldsymbol{c}) + \frac{1}{2N} D_i(\boldsymbol{c}) \partial^2_{c_i} u(\boldsymbol{c}) \Big), \qquad (38)$$

with the deterministic drifts $v_i(\boldsymbol{c})$ and diffusion coefficients $D_i(\boldsymbol{c})$ given by Eqs. (18)-(21). The absorbing boundaries corresponding to the fixation of species 1 and of species 2 impose the boundary conditions $u(c_1, 0) = 1$ and $u(0, c_2) = 0$, respectively. Eq. (38) does not admit an exact solution, and (as mentioned above) the standard technique of escape from a potential well can not be applied since $v_i(\boldsymbol{c})$ is not a gradient of a potential function, i.e., $|\vec{\nabla} \times \vec{v}(\boldsymbol{c})| = |\mu_1(1-\beta_1)c_1 - \mu_2(1-\beta_2)c_2| \neq 0$. Despite these complications, given an empirical data set with a plateau structure of fixation probability *a priori*, we can solve for $u(\boldsymbol{c})$ accurate to first order in $1/N$ by the method of matched asymptotic expansions [50–53]. The strategy is to separately find asymptotic solutions of $u(\boldsymbol{c})$ in the plateau region and in the boundary layers adjacent to the absorbing boundaries, and then perform asymptotic matching of the local solutions. Note that our analysis follows from the Fokker-Planck approximation to the Master equation. It has been shown for initial conditions *starting from a metastable state*, for example in Refs. [38, 54, 55], that the quasi-stationary distribution (QSD) and the mean fixation time when fixations occur via rare fluctuations are accurately predicted by the WKB approximation of the Master equation, rather than by the WKB approximation of the Fokker-Planck approximation. However, the functional form of the QSD and of the mean fixation time from the two methods coincide, and are given by Eq. (C2) and Eq. (48) respectively. We show here that treating the N-independent parameters in the functional form as fitting parameters yields excellent fits to the plateau fixation probability and the plateau mean fixation time caused by escape from a QSD. The utility of the Fokker-Planck approximation here is its ability to predict *crossover behaviors* from the boundary values to the plateau values of the fixation probability and the mean fixation time from asymptotic expansions in $1/N$. As discussed in Sec. IV A, these crossovers are the essential feature of strong mutualism with varying population sizes and, to the best of our knowledge, have not been calculated previously by any technique. With the crossover behaviors in mind, we proceed with the usual Fokker-Planck approximation of the Master equation.

In the plateau region, the fixation probability $u(\boldsymbol{c})$ near the coexistence fixed point $\boldsymbol{c}^* = (c_1^*, c_2^*)$ is approximately equal to $P \equiv u(\boldsymbol{c}^*)$. Similar to strong mutualism with a fixed population size, the dynamics in the plateau region can be characterized by a rapid approach to the coexistence fixed point $\boldsymbol{c}^*$ before weak fluctuations eventually drive the system toward fixation by a large deviation. Eq. (38) guarantees the existence of the plateau structure if number fluctuations are sufficiently weak. Indeed, in the limit $1/N \to 0$, Eq. (38) reduces to the simple advection equation $0 = \sum_{i=1}^{2} v_i(\boldsymbol{c})\partial_{c_i} u(\boldsymbol{c})$. The associated characteristics $\boldsymbol{c}(t)$ obey the mean field dynamics $dc_i(t)/dt = v_i(\boldsymbol{c})$ on which $du(\boldsymbol{c}(t))/dt = 0$, meaning that the fixation probability along each characteristic is constant. Because all the characteristics meet at the stable fixed point $\boldsymbol{c}^*$, we conclude $u(\boldsymbol{c}) = P \equiv u(\boldsymbol{c}^*)$. This plateau value, however, can not extend over the entire domain without violating the boundary conditions; hence, boundary layers adjacent to the absorbing boundaries are an essential part of the physics.

Analogous to $u(f^*)$ in the previous subsection, the plateau fixation probability $P \equiv u(\boldsymbol{c}^*)$ is the ratio of the flux into the absorbing boundary $f = 1$ to the total flux into both of the absorbing boundaries $f = 0$ and $f = 1$, see Appendix C. The probability flux peaks at the saddle fixed point of each absorbing boundary, which suggests that these saddle fixed points dominate the most probable escape routes for each absorbing boundary. Appendix C discusses the derivation of the N-dependence of P which takes the asymptotic form similar to Eq. (37):

$$P \approx \frac{1}{1 + e^{-N\Delta S_0 + \Delta S_1}}, \tag{39}$$

where ΔS_0 and ΔS_1 are treated here as fitting parameters. For strong symmetric mutualism with $s_o = 0$ and $\beta_1 = \beta_2$, the dynamics has a reflection symmetry with respect to the line $f = 1/2$ in the c_1-c_2 plane; hence, fixation of either species is equally likely and $P = 1/2$ independent of N. In the symmetric case, we can thus infer $\Delta S_0 = \Delta S_1 = 0$. For strong asymmetric mutualism, we expect that, in the limit $N \gg 1$, species 1 is more likely to be fixed if $f^* > 1/2$, and hence $\Delta S_0 > 0$. This assertion is confirmed by simulations in Fig. 7 where we find $\Delta S_0 > 0$ for $f^* > 1/2$ from fitting to Eq. (39). Extrapolations of fits to Eq. (39) imply that if $f^* > 1/2$, then species 1 will be fixed with probability 1 in the limit $N \to \infty$.

In the boundary layers (see Fig. 6), $u(\boldsymbol{c})$ crosses over from the boundary condition values to the plateau value. This crossover embodies two different types of dynamics: fixation at early times without falling into the basin of attraction of $\boldsymbol{c}^*$ and fixation by a large deviation after captured by $\boldsymbol{c}^*$. Fixation at early times is possible if the initial condition lies within the boundary layers, whose characteristic width is $1/N \ll 1$. The characteristic widths and the behavior of crossovers can be extracted by the method of matched asymptotic expansions [50–53]. The details of matched asymptotic expansions are given by Appendix B.

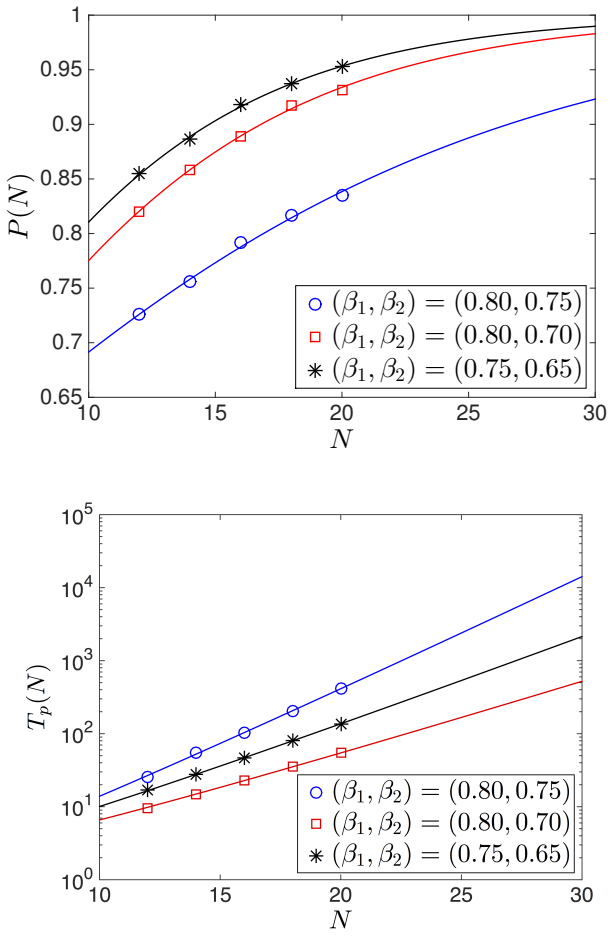

FIG. 7. (Color online) Extrapolations of the plateau fixation probability P (top) based on Eq. (39), and a semilog plot of the plateau mean fixation time T_p (bottom) based on Eq. (48), by best fits to simulations with $N = 12, 14, 16, 18, 20$ in different cases of slightly asymmetric strong mutualism. Symbols are simulation results and solid lines are best fitted curves based on Eqs. (39) and (48). The coexistence fixed point lies closer to the fixation of species 1, yielding $\Delta S_0 > 0$. The plateau fixation probability P increases at increasing N and saturates at 1 as $N \to \infty$. Note that the plateau mean fixation time T_p grows exponentially with N.

In the boundary layer adjacent to the absorbing boundary $c_2 = 0$ and away the absorbing boundary $c_1 = 0$, the asymptotic large N form of the fixation probability reads

$$u(\boldsymbol{c}) = P + (1 - P)e^{-Nc_2/\Phi_1(c_1)}, \tag{40}$$

where the function $\Phi_1(x)$ satisfies

$$\begin{aligned} 0 =& -x(1-x)\Phi_1'(x) + (1+s_o)^{-1}[1-(1-\beta_2)x]\Phi_1(x) \\ & -\frac{1}{2}(1+s_o)^{-1}[1+(1-\beta_2)x], \end{aligned} \tag{41}$$

with the matching condition $\lim_{x\to 1}\Phi_1(x) = \frac{2-\beta_2}{2\beta_2}$. For a fixed c_1, Eq. (40) implies that the fixation probability

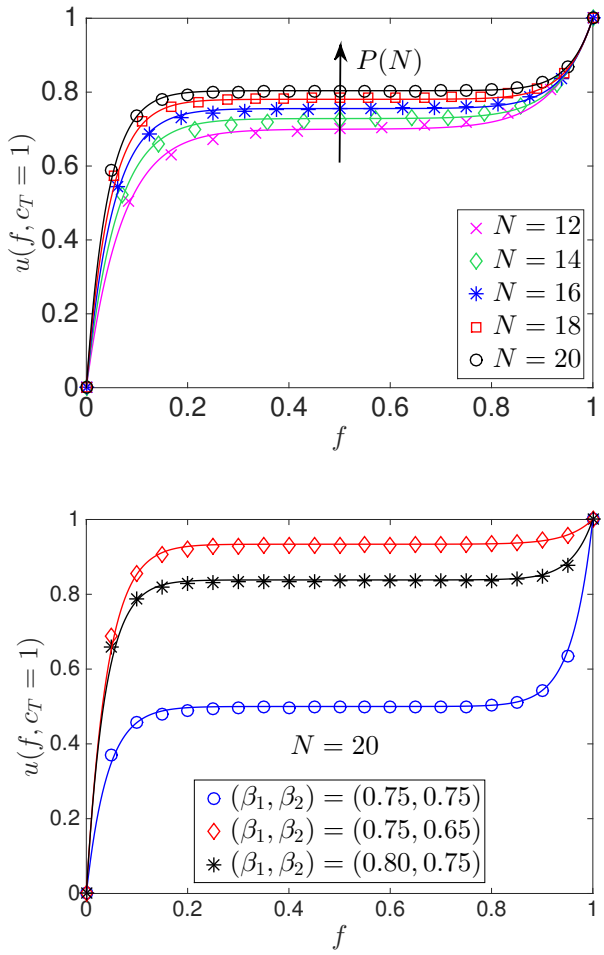

FIG. 8. (Color online) Comparisons between the predicted fixation probability (solid lines) and simulation results (symbols). The plateau fixation probabilities P are determined by fitting Eq. (39) to simulations with $N = 12, 14, 16, 18, 20$ with other parameters fixed. Top: the fixation probability for $s_o = 0, \beta_1 = 0.75, \beta_2 = 0.70$ at increasing N, indicated by the arrow. The matched asymptotics yield excellent estimates for the crossovers from the boundary values to the plateau value $P(N)$ even for N as small as 12. As N increases, the plateau region becomes more elongated (i.e., the boundary layers have characteristic width $1/N$) while the plateau value $P(N)$ increases and eventually saturates at 1 as $N \to \infty$, similar to Fig. 7(top). Bottom: the fixation probability at $N = 20$ for different cases of strong mutualism. Note the improved agreement between simulation and theory compared to Fig. 5.

exhibits a crossover from 1 to P as c_2 increases from $c_2 = 0$ to $c_2 \gg 1/N$. The details of the crossover depend on $1/\Phi_1(x)$, which is a monotonically decreasing function of x for $\beta_1 < 1$ and $\beta_2 < 1$, with $1/\Phi_1(0) = 2$.

In the complementary boundary layer adjacent to the absorbing boundary $c_1 = 0$ and away from the absorbing boundary $c_2 = 0$, the asymptotic form of the fixation probability reads

$$u(\boldsymbol{c}) = P - Pe^{-Nc_1/\Phi_2(c_2)}, \tag{42}$$

where the function $\Phi_2(x)$ satisfies

$$\begin{aligned} 0 =& -x(1-x)\Phi_2'(x) + (1+s_o)[1-(1-\beta_1)x]\Phi_2(x) \\ & -\frac{1}{2}(1+s_o)[1+(1-\beta_1)x], \end{aligned} \tag{43}$$

with the matching condition $\lim_{x\to 1}\Phi_2(x) = \frac{2-\beta_1}{2\beta_1}$. For a fixed c_2, Eq. (42) implies that the fixation probability exhibits a crossover from 0 to P as c_1 increases from $c_1 = 0$ to $c_1 \gg 1/N$. Similar to $1/\Phi_1(x)$, $1/\Phi_2(x)$ is a monotonically decreasing function of x in the parameter range of interest with $1/\Phi_2(0) = 2$.

The above local behaviors of fixation probability can be combined into the global asymptotic solution

$$u(\boldsymbol{c}) = P + (1-P)e^{-Nc_2/\Phi_1(c_1)} - Pe^{-Nc_1/\Phi_2(c_2)}, \tag{44}$$

where the functions $\Phi_1(c_1)$ and $\Phi_2(c_2)$ obey Eq. (41) and Eq. (43) with the associated matching conditions. This global asymptotic solution valid everywhere on the domain except in the small box near the origin $[0, 1/N]\times[0, 1/N]$ where the two boundary layers overlap. Upon changing the coordinate to (f, c_T) to emphasize the important population size degree of freedom, we obtain, finally,

$$\begin{aligned} u(f, c_T) = P &+ (1-P)e^{-N(1-f)c_T/\Phi_1(fc_T)} \\ & - Pe^{-Nfc_T/\Phi_2((1-f)c_T)}. \end{aligned} \tag{45}$$

Fig. 6 summarizes the fixation probability as a function of (c_1, c_2) predicted by Eq. (44) for a strong symmetric mutualism. Fig. 8 shows excellent agreement between the prediction of Eq. (44) and the simulation results for a strong asymmetric mutualism. As expected, the improvements relative to Fig. 5 occur for f near 0 and 1: the boundary behavior missed by the fixed population size model are now well captured even for N as small as 12.

The mean fixation time, $\tau(\boldsymbol{c})$, can also be constructed by the method of matched asymptotic expansions. In this case, we need to solve [33, 34]

$$-1 = \sum_{i=1}^{2}\left(v_i(\boldsymbol{c})\partial_{c_i}\tau(\boldsymbol{c}) + \frac{1}{2N}D_i(\boldsymbol{c})\partial_{c_i}^2\tau(\boldsymbol{c})\right), \tag{46}$$

subject to the boundary conditions $\tau(c_1, 0) = 0$ and $\tau(0, c_2) = 0$. Asymptotic matching arguments similar to Appendix B can be applied to Eq. (46), resulting in the global asymptotic solution for the mean fixation time, namely

$$\tau(\boldsymbol{c}) = T_p\left(1 - e^{-Nc_2/\Phi_1(c_1)} - e^{-Nc_1/\Phi_2(c_2)}\right), \tag{47}$$

where the functions $\Phi_1(c_1)$ and $\Phi_2(c_2)$ still obey Eq. (41) and Eq. (43), and T_p is the plateau mean fixation time

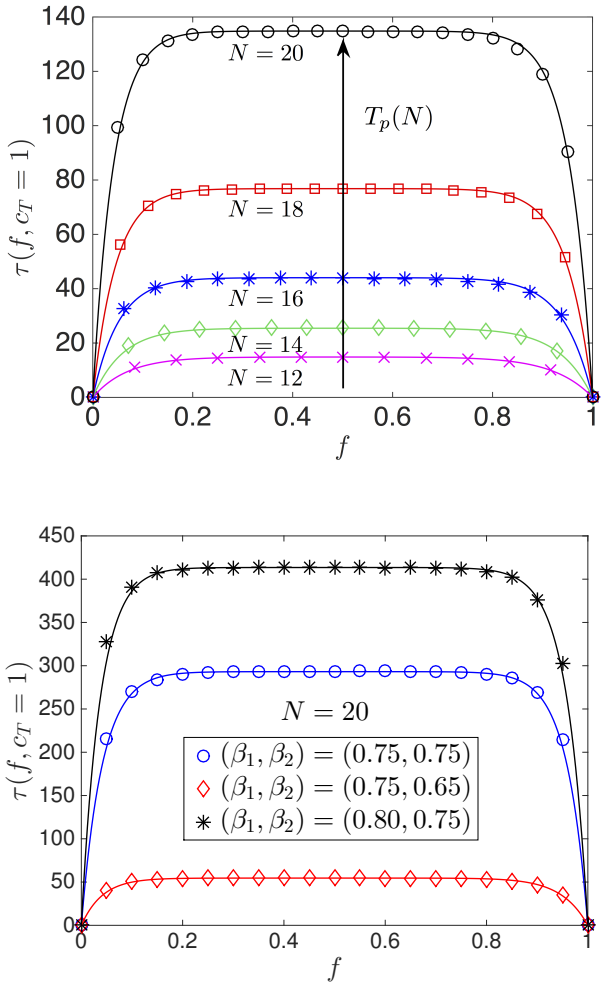

FIG. 9. (Color online). Comparisons between the predicted mean fixation time (solid lines) and simulation results (symbols). Parameters are the same as Fig. 8's. The plateau mean fixation times are determined by fitting, Eq. (48), to simulations with $N = 12, 14, 16, 18, 20$ with other parameters fixed. Top: the mean fixation time for $s_o = 0, \beta_1 = 0.75, \beta_2 = 0.70$ at increasing N. The matched asymptotic expansions yield excellent estimates for the crossovers from the boundary values to the plateau value $T_p(N)$ even for N as small as 12. As N increases, the plateau region becomes more elongated (i.e., the boundary layers have characteristic width $1/N$) while the plateau value $T_p(N)$ grows exponentially similar to Fig. 7(bottom). Bottom: the mean fixation time at $N = 20$ for different cases of strong mutualism.

for the initial condition at the coexistence fixed point. The function $\tau(\boldsymbol{c})$ possesses a plateau structure in which $\tau(\boldsymbol{c}) \approx \tau(\boldsymbol{c}^*) = T_p$, similar to the profile of $u(\boldsymbol{c})$. Furthermore, crossovers from the boundary conditions to T_p are characterized by the same exponentials $e^{-Nc_2/\Phi_1(c_1)}$ and $e^{-Nc_1/\Phi_2(c_2)}$ as in Eq. (44). In the limit $N \gg 1$, the behavior of T_p is exponential in N,

$$T_p \approx \sigma_0 e^{N\sigma_1}, \tag{48}$$

where we treat σ_0 and σ_1 as fitting parameters [50, 56, 57]. Fig. 7(bottom) confirms the exponential scaling of Eq. (48), while Fig. 9 reveals excellent agreement between Eq. (47) and the simulation results. To again emphasize the importance of the population size degree of freedom, we rewrite Eq. (47) in the coordinates (f, c_T) as

$$\tau(f, c_T) = T_p\Big(1 - e^{-N(1-f)c_T/\Phi_1(fc_T)} - e^{-Nfc_T/\Phi_2((1-f)c_T)}\Big). \tag{49}$$

V. CONCLUSIONS

We have explored the interplay between evolutionary dynamics and population dynamics in a well-mixed competitive Lotka-Volterra model in various limits. The model gives rise to 5 different scenarios, similar to evolutionary game theory, without however fixing the overall population size, thereby demonstrating an explicit microscopic system exhibiting the feedback between evolutionary dynamics and population dynamics phenomenologically studied in Refs. [58, 59].

In the limit $|\beta_1| \ll 1$, $|\beta_2| \ll 1$, and $1/N \ll 1$, with an arbitrary reproductive advantage near the origin s_o, describes rapid relaxational dynamics of population size toward a *fixed* equilibrium size along a quasi-deterministic growth trajectory on which $\rho \equiv (1-f)f^{-1/(1+s_o)}c_T^{s_o/(1+s_o)}$ is constant. The variable ρ relates the population frequency f to the total population size c_T as c_T approaches the quasi-equilibrium at $c_T \approx 1$: The frequency of a reproductively advantageous species, on average, increases as dilute populations ($c_T < 1$) grow, and decreases as overcrowded populations ($c_T > 1$) decline. For $s_o = 0$, replicator dynamics with genetic drift is recovered when $c_T \approx 1$, despite population size fluctuations away from $c_T = 1$. Only in this limit is the dynamics near the equilibrium population size a simple generalization of conventional population genetics without mutation with an independently fluctuating population size. From the perspective of equilibrium statistical mechanics, this simple limit is analogous to the generalization from a canonical ensemble to a grand canonical ensemble in the thermodynamic limit [30]. However, for $s_o \neq 0$, population size fluctuations couple to evolutionary dynamics in a nontrivial fashion and replicator dynamics with genetic drift is no longer an appropriate description. Our results demonstrate explicitly a circumstance such that the fixed effective population size model in population genetics is incomplete.

It would be interesting to study how population size fluctuations affect evolutionary dynamics near a fixed equilibrium population size when $s_o \neq 0$ in selection scenarios other than quasi-neutral evolution studied in Refs. [42–45]. Particularly interesting is the Prisoner's Dilemma briefly discussed at the end of Appendix A. In this case, fluctuation-induced selection can actually op-

pose the usual selection bias in the Prisoner's Dilemma, illustrating a fluctuation-driven mechanism other than genetic drift (or spatial segregation [60]) that can alleviate the dilemma of cooperation [20].

We also studied competitions that take place with a strongly varying population size (as opposed to competition with a nearly fixed population size), as in the strong mutualism limit. Fixation events can now arise via two distinct mechanisms: fixation at long times by rare escape from the strongly attractive coexistence fixed point, and fixation at early times before reaching the neighborhood of the coexistence fixed point. The former situation is typical for initial conditions well away from the absorbing boundaries $(c_1, 0)$ and $(0, c_2)$, where the system initially falls toward the coexistence fixed point, resulting in a plateau of constant fixation probability and a plateau in the mean fixation time. The latter situation arises for initial conditions lying close to the absorbing boundaries where fluctuations can fix one species before falling into the coexistence fixed point. The crossovers from the absorbing boundaries to the plateau in the fixation probability and the mean fixation time can be studied by matched asymptotic expansions, accounting for number fluctuations, evolutionary dynamics, and population dynamics. As shown in Fig. 5, the fixed population size model underestimates the number of fixation events that can occur near the absorbing boundaries, thereby overestimating the probability and duration of species coexistence. This dynamics can be important in the context of range expansions of mutualists [15, 24] where populations at the expanding frontier are continuously subject to interaction in a growing population size, which may alter parameter values separating an active (mutualistic) phase from inactive (single species domination) phase.

Although our analytical predictions from the Fokker-Planck approximation show excellent agreement with numerical simulations of the Master equation, it would be interesting to study strong mutualism from other approaches such as the WKB approximation of the Master equation [38, 54, 55]. These approaches can accurately predict the quasi-stationary distribution and the plateau mean fixation time when fixations occur by large deviations from a metastable state without resorting to fitting parameters of the plateau values. Lastly, the fate of competitions as a function of both population size and the frequency in other competition scenarios with a varying population size under strong selection would also be worth investigating.

ACKNOWLEDGMENTS

We thank Mogens Jensen, Maxim Lavrentovich, Simone Pigolotti, and Melanie Müller for helpful discussions. This work was supported in part by the National Science Foundation (NSF) through grant DMR-1306367, and by the Harvard Materials Research Science and Engineering Center through grant DMR-1420570. Portions of this research were conducted during a stay at the Center for Models of Life at the Niels Bohr Institute, the University of Copenhagen. Computations were performed on the Odyssey cluster supported by the FAS Division of Science, Research Computing Group at Harvard University.

Appendix A: Coupled dynamics of f and c_T

Upon applying Ito's change of variable to Eq. (22) and denoting $\mu = \mu_2$ and $(1+s_o)\mu = \mu_1$ [33, 34], the coupled stochastic dynamics of f and c_T are described by

$$\frac{df}{dt} = \mu v_R(f, c_T) + \mu\left(c_T + \frac{1}{N}\right) v_E(f) + \sqrt{\frac{\mu D_R^{(f)}(f, c_T) + \mu D_E^{(f)}(f)}{N}}\Gamma_f(t), \tag{A1}$$

$$\frac{dc_T}{dt} = \mu(1+s_o f) v_G(c_T) + \mu(\alpha_1+\alpha_2)c_T^2 f(1-f) + \sqrt{\frac{\mu D_R^{(c_T)}(f, c_T) + \mu D_E^{(c_T)}(f, c_T)}{N}}\Gamma_{c_T}(t), \tag{A2}$$

where the N-independent functions in the deterministic drifts and in the strength of an uncorrelated Gaussian white noise with $\langle \Gamma_a(t)\Gamma_b(t')\rangle = \delta_{ab}\delta(t-t')$ and $\langle \Gamma_a(t)\rangle = 0$ are given by

$$v_R(f, c_T) = \left[(1-c_T) - \frac{1}{N}\left(\frac{1+c_T}{c_T}\right)\right] s_o f(1-f), \tag{A3}$$

$$v_E(f) = f(1-f)[\alpha_1 + (\alpha_1+\alpha_2)f], \tag{A4}$$

$$v_G(c_T) = c_T(1-c_T), \tag{A5}$$

$$D_R^{(f)}(f, c_T) = f(1-f)[1+s_o(1-f)]\left(\frac{1+c_T}{c_T}\right), \tag{A6}$$

$$D_E^{(f)}(f) = -f(1-f)[\alpha_1(1-f)^2 + \alpha_2 f^2], \tag{A7}$$

$$D_R^{(c_T)}(f, c_T) = c_T(1+c_T)(1+s_o f), \tag{A8}$$

$$D_E^{(c_T)}(f, c_T) = -(\alpha_1+\alpha_2)c_T^2 f(1-f). \tag{A9}$$

Here, the subscript R denotes a contribution involving the reproductive advantage near the origin s_o, whereas the subscript E denotes the contribution from evolutionary parameters defined in Eq. (13) $\alpha_1 = (1+s_o)\beta_1$ and $\alpha_2 = \beta_2$, and $v_E(f)$ and $v_G(c_T)$ describe the deterministic replicator dynamics and the logistic growth dynamics respectively. The $\mathcal{O}(1/N)$ contributions to the deterministic drift induced by number fluctuations of c_1 and c_2 only appear in df/dt and originate from Ito's change of variable formula [33, 34].

Under the replicator condition ($|\alpha_1| \ll 1$, $|\alpha_2| \ll 1$, and $c_T \approx 1$), we have $\left|D_E^{(f)}/D_R^{(f)}\right| \ll 1$ and

$\left|D_E^{(c_T)}/D_R^{(c_T)}\right| \ll 1$ so we can neglect the contributions from evolutionary parameters in the noise. Therefore, at $s_o = 0$ the equations simplify,

$$\frac{df}{dt} = \mu v_E(f)\left(c_T + \frac{1}{N}\right) + \sqrt{\frac{\mu}{N} f(1-f)\left(\frac{1+c_T}{c_T}\right)}\Gamma_f(t), \tag{A10}$$

$$\frac{dc_T}{dt} = \mu v_G(c_T) + \mu\,(\beta_1+\beta_2)c_T^2 f(1-f) + \sqrt{\frac{\mu}{N} c_T(1+c_T)}\Gamma_{c_T}(t). \tag{A11}$$

When $c_T \approx 1$, (A10) reduces to Eq. (23) and (A11) reduces to Eq. (24) in the limit $|\beta_1+\beta_2| \ll 1/N \ll 1$.

For $s_o \neq 0$ and $1/N \ll 1$, the coupled stochastic dynamics when $c_T \approx 1$ acquires contributions from the reproductive advantage near the origin s_o. The dynamics is now described by

$$\frac{df}{dt} = \mu v_R(f,c_T) + \mu c_T v_E(f) + \sqrt{\frac{\mu}{N} f(1-f)[1+s_o(1-f)]\left(\frac{1+c_T}{c_T}\right)}\Gamma_f(t), \tag{A12}$$

$$\frac{dc_T}{dt} = \mu(1+s_o f)v_G(c_T) + \mu(\alpha_1+\alpha_2)c_T^2 f(1-f) + \sqrt{\frac{\mu}{N} c_T(1+c_T)(1+s_o f)}\Gamma_{c_T}(t). \tag{A13}$$

In quasi-neutral evolution ($\alpha_1 = \alpha_2 = 0$), the dynamics of f on the equilibrium line $c_T = 1$ acquires the fluctuation-induced selection term $v_R(f, c_T = 1) = -2s_o f(1-f)/N$, which actually favors the fixation of the species with a reproductive *disadvantage* near the origin ($s_0 < 0$). The presence of non-vanishing deterministic drift is in stark contrast to the unbiased random walk behavior of neutral evolution along the equilibrium line displayed in Eq.(30).

Another interesting limit also arises when $\alpha_1 = -\alpha_2 \sim \mathcal{O}(s_o/N)$, where the fluctuation-induced selection term $\mu v_R(f, c_T = 1) = -(2\mu s_o/N)f(1-f)$ can compete with the usual fixed population size selection strength $\mu v_E(f) = \mu\alpha_1 f(1-f)$ and the genetic drift $D_R^{(f)}(f, c_T = 1) = (2\mu/N)f(1-f)[1+s_o(1-f)]$. In this case, fluctuation-induced selection can oppose the standard selection in population genetics, or equivalently in the Prisoner's Dilemma of evolutionary game theory, and thus influence the dilemma of cooperation.

Appendix B: Matched asymptotics for strong mutualism with a varying population size

In this appendix, we construct the fixation probability for strong mutualism from the method of matched asymptotic expansions, or equivalently the boundary layer method, discussed in [50–53]. First, consider the asymptotic large N solution $u(c_1, c_2)$ of the backward Kolmogorov equation (38) near the saddle fixed points. In the neighborhood of the fixed point $(0,1)$, we introduce the stretched coordinates $\eta_1 = c_1 N$ and $\eta_2 = (c_2-1)\sqrt{N}$, and rewrite the fixation probability in the new coordinates as $U(\eta_1,\eta_2) = u(\eta_1/N, 1+\eta_2/\sqrt{N})$. Upon neglecting the terms of $\mathcal{O}(1/\sqrt{N})$, Eq. (38) in the new coordinates reads

$$0 = \mu_1\beta_1\eta_1\partial_{\eta_1}U + \Big(\frac{\mu_1+\mu_2}{2} - \frac{\mu_1\beta_1}{2}\Big)\eta_1\partial_{\eta_1}^2 U - \mu_2\eta_2\partial_{\eta_2}U + \mu_2\partial_{\eta_2}^2 U. \tag{B1}$$

Separation of variables $U(\eta_1,\eta_2) = X_1(\eta_1)X_2(\eta_2)$ reduces Eq. (B1) to an eigenvalue problem

$$\lambda X_1 = \Big(\frac{\mu_1+\mu_2}{2} - \frac{\mu_1\beta_1}{2}\Big)\eta_1 X_1'' + \mu_1\beta_1\eta_1 X_1', \tag{B2}$$

$$-\lambda X_2 = \mu_2 X_2'' - \mu_2\eta_2 X_2', \tag{B3}$$

where λ is an eigenvalue. The general solution to (B3) is

$$X_2(\eta_2) = C_1 H_{\frac{\lambda}{\mu_2}}\left(\frac{\eta_2}{\sqrt{2}}\right) + C_2 {}_1F_1\left(-\frac{\lambda}{2\mu_2}; \frac{1}{2}; \frac{\eta_2^2}{2}\right), \tag{B4}$$

where C_1 and C_2 are constants, $H_n(z)$ is the Hermite polynomial, and ${}_1F_1(a;b;z)$ is the confluent hypergeometric function of the first kind. The matching condition to the plateau fixation probability $U(\eta_1 \to \infty, \eta_2) = P$ enforces $X_2(\eta_2)$ to be a constant. This is possible only when $C_2 = 0$ and $\lambda = 0$ so $X_2(\eta_2) = C_1$. Because zero is the only eigenvalue consistent with the matching condition, (B2) reduces to

$$0 = \Big(\frac{\mu_1+\mu_2}{2} - \frac{\mu_1\beta_1}{2}\Big)\eta_1 X_1'' + \mu_1\beta_1\eta_1 X_1', \tag{B5}$$

whose general solution is

$$X_1(\eta_1) = B_1 - B_2\Big(\frac{\mu_1+\mu_2}{2\mu_1\beta_1} - \frac{1}{2}\Big)e^{-\eta_1\mu_1\beta_1/(\mu_1+\mu_2-\mu_1\beta_1)}, \tag{B6}$$

where B_1 and B_2 are constants. By imposing the boundary condition $U(0,\eta_2) = 0$ and the matching condition $U(\eta_1 \to \infty, \eta_2) = P$, it follows that the fixation probability in the original coordinates valid in the vicinity of the fixed point $(0,1)$ is

$$u(\boldsymbol{c}) = P + Pe^{-Nc_1[2\beta_1/(2-\beta_1)]}. \tag{B7}$$

A similar argument can be applied to the asymptotic solution near the fixed point $(1,0)$. In this case, the stretched coordinates are $\eta_1 = (c_1-1)\sqrt{N}$ and $\eta_2 = c_2 N$, with the fixation probability in the new coordinates given by $U(\eta_1,\eta_2) = u(1+\eta_1/\sqrt{N}, \eta_2/N)$. Eq. (38) in the new coordinates, with terms of $\mathcal{O}(1/\sqrt{N})$ neglected, reads

$$0 = -\mu_1\eta_1\partial_{\eta_1}U + \mu_1\partial_{\eta_1}^2 U + \mu_2\beta_2\eta_2\partial_{\eta_2}U + \Big(\frac{\mu_1+\mu_2}{2} - \frac{\mu_2\beta_2}{2}\Big)\eta_2\partial_{\eta_2}^2 U, \tag{B8}$$

which is equivalent to (B1) with indices 1 and 2 interchanged. Following the method of separation of variables as above and imposing the boundary condition $U(\eta_1, 0) = 1$ as well as the matching condition $U(\eta_1, \eta_2 \to \infty) = P$, we arrive at the fixation probability valid in the vicinity of the fixed point $(1, 0)$

$$u(\boldsymbol{c}) = P + (1 - P)e^{-Nc_2[2\beta_2/(2-\beta_2)]}. \tag{B9}$$

Now consider the asymptotic solutions away from the saddle fixed points but still in the boundary layers. In the boundary layer adjacent to the absorbing boundary $c_1 = 0$ but away from the saddle fixed point $(0, 1)$, we introduce the stretched coordinate $\eta_1 = c_1 N$ and $\eta_2 = c_2$. Upon neglecting the contributions of $\mathcal{O}(1/N)$ and rewriting the fixation probability in the new coordinate as $U(\eta_1, \eta_2) = u(\eta_1/N, \eta_2)$, Eq. (38) becomes

$$\begin{aligned} 0 = {} & 2\mu_2\eta_2(1 - \eta_2)\partial_{\eta_2}U + 2[\mu_1 - (\mu_1 - \mu_1\beta_1)\eta_2]\eta_1\partial_{\eta_1}U \\ & + [\mu_1 - (\mu_1 + \mu_1\beta_1)\eta_2]\eta_1\partial^2_{\eta_1}U. \end{aligned} \tag{B10}$$

We can turn (B10) into a separable PDE and solve the associated eigenvalue problem by transforming to the new coordinates $x_1 = \eta_1/\Phi_2(\eta_2)$, and $x_2 = \eta_2$. Substituting the coordinate transformation $V(x_1, x_2) = U(x_1\Phi_2(x_2), x_2)$ into (B10), we find $V(x_1, x_2)$ satisfies a separable PDE

$$\begin{aligned} 0 = {} & x_1\partial^2_{x_1}V + x_1\partial_{x_1}V \\ & + 2\frac{\mu_2}{\mu_1}\Big[\frac{x_2(1 - x_2)}{1 - (1 + \beta_1)x_2}\Phi_2(x_2)\Big]\partial_{x_2}V, \end{aligned} \tag{B11}$$

with $\Phi_2(x)$ obeys the first order differential equation given in Eq (43). Separation of variables $V(x_1, x_2) = V_1(x_1)V_2(x_2)$ turns (B11) into an eigenvalue problem

$$\lambda V_1 = x_1V_1'' + x_1V_1', \tag{B12}$$

$$-\lambda V_2 = 2\frac{\mu_2}{\mu_1}\Big[\frac{x_2(1 - x_2)}{1 - (1 + \beta_1)x_2}\Phi_2(x_2)\Big]V_2', \tag{B13}$$

with λ the eigenvalue. Again, matching to the fixation probability at the plateau $U(\eta_1 \to \infty, \eta_2) = P$ enforces $V_2(x_2)$ to be constant which is possible only if $\lambda = 0$. The general solution to (B12) with $\lambda = 0$ is

$$V_1(x_1) = D_1 - D_2e^{-x_1}. \tag{B14}$$

Upon imposing the boundary condition $U(0, \eta_2) = 0$ as well as the matching condition $U(\eta_1 \to \infty, \eta_2) = P$, we obtain the fixation probability in the original coordinate valid within the boundary layer adjacent to the absorbing boundary $c_1 = 0$, namely

$$u(\boldsymbol{c}) = P - Pe^{-Nc_1/\Phi_2(c_2)}. \tag{B15}$$

Upon matching (B15) to the asymptotic solution in the vicinity of the saddle fixed point $(1, 0)$, (B9), we find a first order differential equation governing Φ_2, given by Eq. (43), with the matching condition $\lim_{x\to 1}\Phi_2(x) = \frac{2-\beta_1}{2\beta_1}$.

A similar argument with index 1 and 2 interchanged determines the asymptotic solution within the boundary layer adjacent to the absorbing boundary $c_2 = 0$. We find that the fixation probability in this region is given by

$$u(\boldsymbol{c}) = P + (1 - P)e^{-Nc_2/\Phi_1(c_1)}, \tag{B16}$$

where $\Phi_1(x)$ obeys Eq. (41) subject to the matching condition $\lim_{x\to 1}\Phi_1(x) = \frac{2-\beta_2}{2\beta_2}$. Therefore, the global solution with smooth crossovers from the plateau P to the the boundary layer behavior of (B15) and (B16) is given by Eq. (44).

Appendix C: Fixation from a quasi-stationary distribution

The analysis in this section follows the general discussion on the high dimensional exit problem by Grasman and Herwaarden [50]. We first argue that, near the absorbing boundaries, the quasi-stationary distribution (QSD) $p_{st}(\boldsymbol{c})$ is peaked at the saddle fixed point $(0, 1)$ and $(1, 0)$. To see this, consider the (stationary) Fokker-Planck equation

$$0 = \sum_{i=1}^{2}\Big(-\partial_{c_i}v_ip_{st} + \frac{1}{2N}\partial^2_{c_i}D_ip_{st}\Big), \tag{C1}$$

where v_i and D_i are given by Eqs. (18)-(21). When the problem can be regarded as a rare event escape from a metastable state, the asymptotic solution to (C1) is solved by the WKB ansatz [35, 50, 54, 61]

$$p_{st}(\boldsymbol{c}) = w(\boldsymbol{c})e^{-N\Psi(\boldsymbol{c})}. \tag{C2}$$

Substituting (C2) into (C1) and collecting the leading order terms in N leads to an eikonal equation,

$$0 = \sum_{i=1}^{2}\Big(v_i(\partial_{c_i}\Psi) + \frac{1}{2}D_i(\partial_{c_i}\Psi)^2\Big). \tag{C3}$$

Collecting terms of $\mathcal{O}(1)$ results in

$$\begin{aligned} 0 = {} & \sum_{i=1}^{2}\Big(D_i(\partial_{c_i}\Psi) + v_i\Big)\partial_{c_i}w \\ & + \sum_{i=1}^{2}\Big(\frac{1}{2}D_i\partial^2_{c_i}\Psi + (\partial_{c_i}D_i)(\partial_{c_i}\Psi)\Big)w. \end{aligned} \tag{C4}$$

In the neighborhood of the absorbing boundary $c_1 = 0$, we expand Ψ around $c_1 = 0$ as

$$\Psi(\boldsymbol{c}) = \Psi_2^{(0)}(c_2) + \Psi_2^{(1)}(c_2)c_1 + \frac{1}{2}\Psi_2^{(2)}(c_2)c_1^2 + \cdots, \tag{C5}$$

where the subscript 2 of Ψ denotes the expansion around the fixation of species 2 and the superscript labels the order of expansion. Upon substituting the expansion

(C5) into (C3) and collecting terms of $\mathcal{O}(c_1^0)$, we find $\Psi_2'^{(0)}(c_2) = 2(c_2-1)/(c_2+1)$. Therefore, in the limit $c_1 \to 0$, $\Psi(\boldsymbol{c})$ is minimal at $c_2 = 1$, implying that p_{st} is peaked in the neighborhood of the fixed point $(0,1)$ provided $N \gg 1$.

For the behavior of $w(\boldsymbol{c})$ near $(0,1)$, it turns out the singular behavior of w when $c_1 \to 0$ scales as $w \sim 1/c_1$. We refer to the discussion in Ref. [50] for the related problem of extinction probability in the predator-prey model. The singular behavior suggests the QSD is concentrated in the neighborhood of the saddle fixed point.

To extract the quantitative behavior of p_{st} near the saddle fixed point $(0,1)$, we Taylor expand Ψ around $(0,1)$

$$\Psi(\boldsymbol{c}) = \bar{\Psi}_2^{(0)} + \bar{\Psi}_2^{(1)} c_1 + \bar{\Psi}_2^{(2)}(c_2-1) + \frac{1}{2}\bar{\Psi}_2^{(3)}(c_2-1)^2 + \cdots, \tag{C6}$$

where we denote the i^{th} expansion coefficient around the saddle fixed point of species 2 by $\bar{\Psi}_2^{(i)}$. Upon substituting the expansion (C6) into (C3) and (C4) we get $\bar{\Psi}_2^{(1)} = -2\beta_1/(2-\beta_1)$, $\bar{\Psi}_2^{(2)} = 0$, and $\bar{\Psi}_2^{(3)} = 1$. Therefore, in the neighborhood of the fixed point $(0,1)$, the QSD takes the form

$$p_{st}(\boldsymbol{c}) \approx \frac{\bar{w}_2^{(0)} \exp(-N\bar{\Psi}_2^{(0)})}{c_1} \times \exp\left[N\left(\frac{2\beta_1}{2-\beta_1}c_1 - \frac{(c_2-1)^2}{2}\right)\right]. \tag{C7}$$

Similar arguments lead to the behavior of the QSD in the neighborhood of the fixed point $(1,0)$, which reads

$$p_{st}(\boldsymbol{c}) \approx \frac{\bar{w}_1^{(0)} \exp(-N\bar{\Psi}_1^{(0)})}{c_2} \times \exp\left[N\left(\frac{2\beta_2}{2-\beta_2}c_2 - \frac{(c_1-1)^2}{2}\right)\right]. \tag{C8}$$

We now relate the behavior of the QSD near the absorbing boundaries to the plateau fixation probability P in the bulk region by employing the identity resulting from the divergence theorem:

$$\begin{aligned}
&\int_\Omega (p\hat{L}u - u\hat{M}p)dc_1dc_2 \\
&= \int_{\partial\Omega}\Bigg(\sum_{i=1}^{2}\frac{1}{2N}\Big[n_iD_i(p\partial_{c_i}u - u\partial_{c_i}p) - n_i(\partial_{c_i}D_i)pu\Big] \\
&\qquad + \sum_{i=1}^{2} n_i v_i pu\Bigg)dS,
\end{aligned} \tag{C9}$$

where $\hat{L}$ is the backward-Kolmogorov operator, u is the solution to the backward-Kolmogorov equation, $\hat{M}$ is the forward-Kolmogorov (Fokker-Planck) operator, p is the solution to the forward-Kolmogorov equation, Ω is the domain of interest, and n_i is the i^{th} components of the normal vector at the boundary $\partial\Omega$. In the long-time limit when the QSD has already developed, the volume integral (left hand side) of (C9) vanishes since $\hat{L}u = 0$ and $\hat{M}p_{st} = 0$. To evaluate the surface integral in (C9) and avoid the singularity of p_{st} on each absorbing boundary, we consider the domain $\Omega = \{\boldsymbol{c} \mid c_1 > \varepsilon, c_2 > \varepsilon\}$ and evaluate (C9) in the limit $\varepsilon \to 0$. In this domain, (C9) becomes

$$\begin{aligned}
0 =& \int_\varepsilon^\infty dc_2\Bigg(\frac{1}{2N}\big[D_1(p_{st}\partial_{c_1}u - u\partial_{c_1}p_{st}) - (\partial_{c_1}D_1)p_{st}u\big] \\
&\qquad + v_1 p_{st}u\Bigg)_{c_1=\varepsilon} \\
&+ \int_\varepsilon^\infty dc_1\Bigg(\frac{1}{2N}\big[D_2(p_{st}\partial_{c_2}u - u\partial_{c_2}p_{st}) - (\partial_{c_2}D_2)p_{st}u\big] \\
&\qquad + v_2 p_{st}u\Bigg)_{c_2=\varepsilon}.
\end{aligned} \tag{C10}$$

(C10) relates the plateau fixation probability P contained in u by (B7) and (B9) to the boundary behavior of p_{st}. Substituting the asymptotic solutions of the QSD given by (C7) and (C8), the asymptotic solutions of u given by (B7) and (B9), and the deterministic drifts as well as diffusion coefficients given by Eqs. (18)-(21) into (C10), we obtain after taking the limits $\varepsilon \to 0$ and $N \gg 1$

$$\begin{aligned}
0 =& \frac{2\beta_1}{2-\beta_1}\bar{w}_2^{(0)}\exp(-N\bar{\Psi}_2^{(0)}) \\
&\times \int_0^\infty dc_2\Bigg\{\left[-\frac{\mu_1 P}{2} - \frac{\mu_1(1-\beta_1)P}{2}c_2\right] \\
&\qquad \times \exp\left[-\frac{N(c_2-1)^2}{2}\right]\Bigg\} \\
&+ \frac{2\beta_2}{2-\beta_2}\bar{w}_1^{(0)}\exp(-N\bar{\Psi}_1^{(0)}) \\
&\times \int_0^\infty dc_1\Bigg\{\Bigg[\mu_2\left(1 - \frac{2-\beta_2}{2\beta_2} - \frac{P}{2}\right) \\
&\qquad + \mu_2(1-\beta_2)\left(1 + \frac{2-\beta_2}{2\beta_2} - \frac{P}{2}\right)c_1\Bigg] \\
&\qquad \times \exp\left[-\frac{N(c_1-1)^2}{2}\right]\Bigg\}.
\end{aligned} \tag{C11}$$

The integrals can be evaluated by the standard method of Laplace integration when $N \gg 1$. The result reads

$$\begin{aligned}
0 =& \frac{2\beta_1}{2-\beta_1}\bar{w}_2^{(0)}\exp(-N\bar{\Psi}_2^{(0)})\sqrt{\frac{\pi}{N}} \\
&\times \left[-\frac{\mu_1 P}{2} - \frac{\mu_1(1-\beta_1)P}{2}\right] \\
&+ \frac{2\beta_2}{2-\beta_2}\bar{w}_1^{(0)}\exp(-N\bar{\Psi}_1^{(0)})\sqrt{\frac{\pi}{N}} \\
&\times \Bigg[\mu_2\left(1 - \frac{2-\beta_2}{2\beta_2} - \frac{P}{2}\right) \\
&\qquad + \mu_2(1-\beta_2)\left(1 + \frac{2-\beta_2}{2\beta_2} - \frac{P}{2}\right)\Bigg].
\end{aligned} \tag{C12}$$

Upon rewriting $\beta_1 = \mu_1 - \lambda_{12}N$, and $\beta_2 = \mu_2 - \lambda_{21}N$ and

keeping only the leading order term in $1/N$, we obtain the plateau fixation probability

$$P \approx \frac{\lambda_{21}\bar{w}_1^{(0)} e^{-N\bar{\Psi}_1^{(0)}}}{\lambda_{21}\bar{w}_1^{(0)} e^{-N\bar{\Psi}_1^{(0)}} + \lambda_{12}\bar{w}_2^{(0)} e^{-N\bar{\Psi}_2^{(0)}}}. \tag{C13}$$

Recall that $\bar{w}_1^{(0)} e^{-N\bar{\Psi}_1^{(0)}}$ and $\bar{w}_2^{(0)} e^{-N\bar{\Psi}_2^{(0)}}$ are $p_{st}(\boldsymbol{c})$ evaluated at $(1, 0^+)$ and $(0^+, 1)$. Consequently, (C13) is the ratio of the flux into (1,0) to the total flux into (1,0) and (0,1). In the limit $N \gg 1$, (C7) and (C8) imply that, on each absorbing boundary, the QSD peaks up at the saddle fixed point while the width around the peak becomes vanishingly narrow; accordingly, the flux into the saddle fixed point well approximates the flux into the corresponding absorbing boundary. Hence, (C13) describes the ratio of flux into the absorbing boundary at $f = 1$ to the total flux into both the absorbing boundaries at $f = 0$ and $f = 1$.

Note that (C13) can be rewritten in the form similar to Eq. (37) as

$$P \approx \frac{1}{1 + e^{-N\Delta S_0 + \Delta S_1}}, \tag{C14}$$

where $\Delta S_0 \equiv \bar{\Psi}_2^{(0)} - \bar{\Psi}_1^{(0)}$ and $\Delta S_1 \equiv \ln(\lambda_{12}\bar{w}_2^{(0)}) - \ln(\lambda_{21}\bar{w}_1^{(0)})$. Since $\bar{w}_i^{(0)}$ and $\bar{\Psi}_i^{(0)}$ are independent of N, we can vary N while fixing s_o, β_1 and β_2 to infer ΔS_0 and ΔS_1 by fitting the plateau fixation probability P to simulations. In principle, the exact values of ΔS_0 and ΔS_1 may be obtained numerically by simultaneously solving $\bar{w}_i^{(0)}$ and $\bar{\Psi}_i^{(0)}$ from (C3) and (C4) [22, 35, 56, 57], but these are beyond the scope of this work.

[1] S. F. Elena and R. E. Lenski, Nature Reviews Genetics **4**, 457 (2003).
[2] M. M. Desai, Journal of Statistical Mechanics: Theory and Experiment **2013**, P01003 (2013).
[3] L. Dai, D. Vorselen, K. S. Korolev, and J. Gore, Science **336**, 1175 (2012).
[4] A. Sanchez and J. Gore, PLoS biology **11**, e1001547 (2013).
[5] A. S. Griffin, S. A. West, and A. Buckling, Nature **430**, 1024 (2004).
[6] M. A. Nowak, *Evolutionary dynamics: exploring the equations of life* (Harvard University Press, 2006).
[7] E. Frey, Physica A: Statistical Mechanics and its Applications **389**, 4265 (2010).
[8] R. A. Blythe and A. J. McKane, Journal of Statistical Mechanics: Theory and Experiment **2007**, P07018 (2007).
[9] W. J. Ewens, *Mathematical Population Genetics 1: I. Theoretical Introduction* (Springer, 2004), ISBN 0387201912.
[10] J. H. Gillespie, *Population Genetics: A Concise Guide* (JHU Press, 2010), ISBN 1421401703.
[11] D. L. Hartl, A. G. Clark, et al., *Principles of population genetics*, vol. 116 (Sinauer associates Sunderland, 1997).
[12] G. Lambert, S. Vyawahare, and R. H. Austin, Interface focus **4**, 20140029 (2014).
[13] J. M. Smith, *Evolution and the Theory of Games* (Cambridge university press, 1982).
[14] K. S. Korolev and D. R. Nelson, Physical Review Letters **107**, 088103 (2011).
[15] M. J. Müller, B. I. Neugeboren, D. R. Nelson, and A. W. Murray, Proceedings of the National Academy of Sciences **111**, 1037 (2014).
[16] M. Kimura, *The neutral theory of molecular evolution* (Cambridge University Press, 1984).
[17] K. Korolev, M. Avlund, O. Hallatschek, and D. R. Nelson, Reviews of modern physics **82**, 1691 (2010).
[18] M. Kimura, Genetics **47**, 713 (1962).
[19] P. A. P. Moran et al., The statistical processes of evolutionary theory. (1962).
[20] J. Cremer, T. Reichenbach, and E. Frey, New Journal of Physics **11**, 093029 (2009).
[21] M. Mobilia and M. Assaf, EPL (Europhysics Letters) **91**, 10002 (2010).
[22] M. Assaf and M. Mobilia, Journal of Statistical Mechanics: Theory and Experiment **2010**, P09009 (2010).
[23] M. Lassig, arXiv preprint cond-mat/0206093 (2002).
[24] M. O. Lavrentovich and D. R. Nelson, Physical Review Letters **112**, 138102 (2014).
[25] M. O. Lavrentovich, K. S. Korolev, and D. R. Nelson, Physical Review E **87**, 012103 (2013).
[26] G. E. Hutchinson, American Naturalist pp. 137–145 (1961).
[27] T. Tél, A. de Moura, C. Grebogi, and G. Károlyi, Physics Reports **413**, 91 (2005).
[28] P. Perlekar, R. Benzi, D. R. Nelson, and F. Toschi, Physical Review Letters **105**, 144501 (2010).
[29] S. Pigolotti, R. Benzi, M. H. Jensen, and D. R. Nelson, Physical Review Letters **108**, 128102 (2012).
[30] S. Pigolotti, R. Benzi, P. Perlekar, M. H. Jensen, F. Toschi, and D. Nelson, Theoretical Population Biology **84**, 72 (2013).
[31] K. S. Korolev, PLoS computational biology **9**, e1002994 (2013).
[32] R. Pearl and L. Slobodkin, Quarterly Review of Biology pp. 6–24 (1976).
[33] N. G. Van Kampen, *Stochastic processes in physics and chemistry*, vol. 1 (Elsevier, 1992).
[34] C. Gardiner, *Handbook of stochastic processes* (Springer, 1985).
[35] M. Dykman, E. Mori, J. Ross, and P. Hunt, The Journal of Chemical Physics **100**, 5735 (1994).
[36] H. Risken, *Fokker-Planck Equation* (Springer, 1984).
[37] J. Langer, Annals of Physics **54**, 258 (1969).
[38] O. Ovaskainen and B. Meerson, Trends in ecology and evolution **25**, 643 (2010).
[39] J. F. Crow, M. Kimura, et al., *An introduction to population genetics theory.* (New York, Evanston and London: Harper & Row, Publishers, 1970).
[40] M. Kimura and T. Ohta, Genetics **61**, 763 (1969).
[41] G. W. A. Constable and A. J. McKane, Physical Review Letters **114**, 038101 (2015).

[42] T. L. Parsons and C. Quince, Theoretical Population Biology **72**, 468 (2007).
[43] T. L. Parsons, C. Quince, and J. B. Plotkin, Theoretical Population Biology **74**, 302 (2008).
[44] O. Kogan, M. Khasin, B. Meerson, D. Schneider, and C. R. Myers, Physical Review E **90**, 042149 (2014).
[45] Y. T. Lin, H. Kim, and C. R. Doering, Journal of Statistical Physics **148**, 647 (2012).
[46] H. Kleinert, *Path integrals in quantum mechanics, statistics, polymer physics, and financial markets* (World Scientific, 2009).
[47] A. Altland and B. D. Simons, *Condensed matter field theory* (Cambridge University Press, 2010).
[48] D. T. Gillespie, Journal of Computational Physics **22**, 403 (1976).
[49] D. T. Gillespie, The Journal of Physical Chemistry **81**, 2340 (1977).
[50] J. Grasman and O. A. Herwaarden, *Asymptotic methods for the Fokker-Planck equation and the exit problem in applications* (Springer, 1999).
[51] F. Verhulst, *Methods and applications of singular perturbations: boundary layers and multiple timescale dynamics* (Springer, 2006).
[52] C. M. Bender and S. A. Orszag, *Advanced mathematical methods for scientists and engineers I: Asymptotic methods and perturbation theory*, vol. 1 (Springer, 1999).
[53] E. Hinch, *Perturbation methods. 1991.*
[54] M. Assaf and B. Meerson, Physical Review E **81**, 021116 (2010).
[55] D. A. Kessler and N. M. Shnerb, Journal of Statistical Physics **127**, 861 (2007).
[56] V. Elgart and A. Kamenev, Physical Review E **70**, 041106 (2004).
[57] A. Kamenev and B. Meerson, Physical Review E **77**, 061107 (2008).
[58] A. Melbinger, J. Cremer, and E. Frey, Physical Review Letters **105**, 178101 (2010).
[59] J. Cremer, A. Melbinger, and E. Frey, Physical Review E **84**, 051921 (2011).
[60] J. D. Van Dyken, M. J. Müller, K. M. Mack, and D. M. Michael, Current Biology **23**, 919 (2013).
[61] R. Graham and T. Tél, Physical Review A **31**, 1109 (1985).